

# GIANT: Globally Improved Approximate Newton Method for Distributed Optimization

**Shusen Wang**

*shusen@berkeley.edu*

*International Computer Science Institute and Department of Statistics*

*University of California at Berkeley*

*Berkeley, CA 94720, USA*

**Farbod Roosta-Khorasani**

*fred.roosta@uq.edu.au*

*School of Mathematics and Physics*

*University of Queensland*

*St Lucia, QLD 4072, Australia*

**Peng Xu**

*pengxu@stanford.edu*

*Institute for Computational and Mathematical Engineering*

*Stanford University*

*Stanford, CA 94305, USA*

**Michael W. Mahoney**

*mmahoney@stat.berkeley.edu*

*International Computer Science Institute and Department of Statistics*

*University of California at Berkeley*

*Berkeley, CA 94720, USA*

March 25, 2025

## Abstract

For distributed computing environments, we consider the canonical machine learning problem of empirical risk minimization (ERM) with quadratic regularization, and we propose a distributed and communication-efficient Newton-type optimization method. At every iteration, each worker *locally* finds an Approximate NewTon (ANT) direction, and then it sends this direction to the main driver. The driver, then, averages all the ANT directions received from workers to form a *Globally Improved ANT* (GIANT) direction. GIANT naturally exploits the trade-offs between local computations and global communications in that more local computations result in fewer overall rounds of communications. GIANT is highly communication efficient in that, for  $d$ -dimensional data uniformly distributed across  $m$  workers, it has 4 or 6 rounds of communication and  $\mathcal{O}(d \log m)$  communication complexity per iteration. Theoretically, we show that GIANT's convergence rate is faster than first-order methods and existing distributed Newton-type

methods. From a practical point-of-view, a highly beneficial feature of GIANT is that it has only one tuning parameter—the iterations of the local solver for computing an ANT direction. This is indeed in sharp contrast with many existing distributed Newton-type methods, as well as popular first order methods, which have several tuning parameters, and whose performance can be greatly affected by the specific choices of such parameters. In this light, we empirically demonstrate the superior performance of GIANT compared with other competing methods.

**Keywords:** Distributed Optimization, Newton’s Method, Randomized Linear Algebra, Communication Efficient Optimization

## 1. Introduction

The large-scale nature of many modern “big-data” problems, arising routinely in science, engineering, financial markets, Internet and social media, etc., poses significant computational as well as storage challenges for machine learning procedures. For example, the scale of data gathered in many applications nowadays typically exceeds the memory capacity of a single machine, which, in turn, makes learning from data ever more challenging. In this light, several modern distributed computing architectures, e.g., MapReduce (Dean and Ghemawat, 2008), Apache Spark (Zaharia et al., 2010, Meng et al., 2016), GraphLab (Low et al., 2012), and Parameter Server (Li et al., 2014), have been designed to operate on and learn from data at massive scales. Despite the fact that, when compared to a single machine, distributed systems tremendously reduce the storage as well as (local) computational costs, the inevitable cost of communications across the network can often be the bottleneck of distributed computations. As a result, designing methods which can strike an appropriate balance between the cost of computations and that of communications are increasingly desired.

The desire to reduce communication costs is even more pronounced in the *federated learning* framework (Konecny et al., 2016a,b, Bonawitz et al., 2017, McMahan et al., 2017, Smith et al., 2017). Similarly to typical settings of distributed computing, federated learning assumes data are distributed over a network across nodes that enjoy reasonable computational resources, e.g., mobile phones, wearable devices, and smart homes. However, the network has severely limited bandwidth and high latency. As a result, it is imperative to reduce the communications between the center and a node or between two nodes. In such settings, the preferred methods are those which can perform expensive local computations with the aim of reducing the overall communications across the network.

Optimization algorithms designed for distributed environments are abundantly found in the literature. Accelerated gradient methods are embarrassing parallel and easy to implement. Stochastic first-order methods<sup>1</sup>, including distributed variants of stochastic gradient descent (SGD) (Mahajan et al., 2013, Recht et al., 2011, Zinkevich et al., 2010), accelerated SGD (Shamir and Srebro, 2014), variance reduction SGD (Lee et al., 2015, Reddi et al., 2015), substantially reduce the amount of local computations but incur much more communication. Stochastic coordinate descent methods (Fercoq and Richtárik, 2016, Liu et al., 2015, Necoara and Clipici, 2016, Richtárik and Takávc, 2016) and dual coordinate ascent algorithms (Richtárik and Takác, 2016, Yang, 2013, Zheng et al., 2016) are two other

---

1. Those methods that use only gradient information.

classes of first-order algorithms that are suitable for distributed settings but have high communication costs.

The aforementioned methods have very low per-iteration costs, i.e., only a small number of floating point operations (FLOPs) is performed at every iteration. However, this advantage comes at the cost of requiring many iterations to attain reasonable precision. As a result of their highly iterative nature, many of these first-order methods require several rounds of communications and synchronizations in every iteration, and they must do this for many iterations. In a distributed system, due to limitations on the network’s bandwidth and latency, communications across the nodes can oftentimes be the critical bottleneck for the distributed optimization. Such overheads are increasingly exacerbated with the growing number of compute nodes in the network, limiting the scalability of any distributed optimization method that requires many communication-intensive iterations. This has been the main motivation for several methods aiming at reducing communications at the cost of more expensive local computations, e.g., (Devarakonda et al., 2016). However, in these methods, the communication costs have only been reduced by a constant factor. Another approach is to form empirical risk minimization as global variable consensus problems and solve the problem by the alternating direction method of multipliers (ADMM) (Boyd et al., 2011). ADMM decreases the number of communications at the cost of more local computation, which is similar to the spirit of our approach. However, the convergence rate of ADMM is quite slow.

To remedy such draw-backs of high number of iterations for distributed optimization, communication-efficient second-order methods<sup>2</sup> have also been recently considered, e.g., DANE (Shamir et al., 2014), AIDE (Reddi et al., 2016), DiSCO (Zhang and Lin, 2015), and CoCoA (Jaggi et al., 2014, Ma et al., 2015, Smith et al., 2016).<sup>3</sup> (For a detailed discussion of second-order methods and their usefulness in machine learning, see Roosta-Khorasani and Mahoney (2016a,b), Xu et al. (2017a,b) and references therein.) The common-denominator in most of these methods is that they intend to increase the local computations with the aim of reducing the overall iterations, and hence, lowering the amount of communications. In other words, many of these methods are designed to perform as much local computations as possible before making any communications across the network. In doing so, each worker first locally solves a subproblem using its local data. This is then followed by aggregating (e.g., averaging) the local solutions using one round of communication. Pursuing similar objectives, in this paper, we propose a Globally Improved Approximate NewTon (GIANT) method and establish its theoretical convergence properties which demonstrate substantial improvements over other similar second-order methods. We also showcase the superior empirical performance of GIANT through several numerical experiments.

The rest of this paper is organized as follows. In the remainder of this introduction, we summarize our main results: in Section 1.1, we briefly review the empirical risk minimization problem; in this context, in Section 1.2, we give an overview of our proposed Algorithm; our main theoretical results are summarized in Section 1.3; and then, in Section 1.4, we provide a comparison with prior work. Section 2 then gathers some preliminary materials such as notation used throughout this paper as well as a brief review of matrix sketching

---

2. Those methods that, in addition to the gradient, incorporate curvature information.

3. CoCoA works by iteratively forming local *quadratic* approximations to a dual objective function. Thus CoCoA can be thought of as a second-order method.

and Newton’s method. Section 3 presents the details of our proposed algorithm, GIANT. Section 4 then describes GIANT’s main theoretical convergence properties; and extensive numerical experiments are given in Section 5. Finally, concussions and further thoughts are gathered in Section 6. All proofs are deferred to Appendix.

### 1.1 Problem Formulation

In this paper, we consider the distributed variant of empirical risk minimization, a supervised-learning problem arising very often in machine learning and data analysis (Shalev-Shwartz and Ben-David, 2014). More specifically, let  $\mathbf{x}_1, \dots, \mathbf{x}_n \in \mathbb{R}^d$  be the input feature vectors and  $y_1, \dots, y_n \in \mathbb{R}$  be the corresponding response. The goal of supervised learning is to compute a model from the training data, which can be achieved by minimizing an empirical risk function, i.e.,

$$\min_{\mathbf{w} \in \mathbb{R}^d} \left\{ f(\mathbf{w}) \triangleq \frac{1}{n} \sum_{j=1}^n f_j(\mathbf{w}) \right\}, \quad \text{where } f_j(\mathbf{w}) \triangleq l_j(\mathbf{w}^T \mathbf{x}_j) + \frac{1}{2} \mathbf{w}^T \mathbf{M} \mathbf{w}, \quad (1)$$

where  $l_j : \mathbb{R} \mapsto \mathbb{R}$  is convex, twice differentiable, and smooth, and where  $\mathbf{M}$  is symmetric positive semi-definite (SPSD). We further assume that  $f$  is strongly convex, which in turn, implies the uniqueness of the solution to (1). Note that  $y_j$  is implicitly captured by  $l_j$ . Examples of the loss function,  $l_j$ , appearing in (1) include

$$\begin{aligned} \text{linear regression:} & \quad l_j(z_j) = \frac{1}{2}(z_j - y_j)^2, \\ \text{logistic regression:} & \quad l_j(z_j) = \log(1 + e^{-z_j y_j}). \end{aligned}$$

For the regularization term,  $\mathbf{M}$  can be set to all-zero matrix (only if the loss function is strongly convex),  $\gamma \mathbf{I}_d$  for some  $\gamma \geq 0$ , a diagonal matrix with non-negative entries, or some sparse matrix which can be efficiently transferred across the network by message passing.

We consider solving (1) in the regimes where  $n \gg d$ . We assume that the data points,  $\{\mathbf{x}_i\}_{i=1}^n$  are partitioned among  $m$  machines, with possible overlaps, such that the number of local data is larger than  $d$ . Otherwise, if  $n \ll d$ , we can consider the dual problem and partition features. If the dual problem is also decomposable, smooth, strongly convex, and unconstrained, then our approach directly applies. For example, the dual of ridge regression enjoys such properties.

### 1.2 Algorithm Description

Here we describe GIANT and analyze its time and communication complexities. The operations of GIANT in the  $t$ -th iteration are performed in the following way. First, the full gradient  $\mathbf{g}_t \in \mathbb{R}^d$  is computed by summing up all the local gradients. Second, the  $i$ -th local machine, for  $i = 1$  to  $m$ , uses the full gradient  $\mathbf{g}_t$  and its local Hessians  $\tilde{\mathbf{H}}_{t,i} \in \mathbb{R}^{d \times d}$  to compute a local Approximate NewTon (ANT) direction

$$\tilde{\mathbf{p}}_{t,i} \approx \operatorname{argmin}_{\mathbf{p} \in \mathbb{R}^d} \left\| \tilde{\mathbf{H}}_{t,i} \mathbf{p} - \mathbf{g}_t \right\|_2^2.$$

Third, the main driver aggregates all the  $m$  ANT directions to form a Globally Improved ANT (GIANT) direction  $\tilde{\mathbf{p}}_t = \frac{1}{m} \sum_{i=1}^m \tilde{\mathbf{p}}_{t,i}$ . Last, the driver performs the update  $\mathbf{w}_{t+1} =$

$\mathbf{w}_t - \beta_t \tilde{\mathbf{p}}_t$  and send  $\mathbf{w}_{t+1}$  to the workers. Under the Assumptions made in Section 4, the step size  $\beta_t = 1$  is safe; otherwise,  $\beta_t$  can be determined by backtracking line search.

The per-iteration time complexities of GAIN can be calculated as follows. Assume each worker locally holds  $s$  samples. In the  $t$ -th iteration, each worker can solve  $\tilde{\mathbf{H}}_{t,i} \tilde{\mathbf{p}}_{t,i} = \mathbf{g}_t$  either exactly by matrix inversion (as a theoretical point, obviously not recommended in practice) or inexactly by taking  $q$  ( $\geq 1$ ) conjugate gradient (CG) steps (the choice of  $q$  will be discussed soon). It is easy to see that the time complexity of the former approach is  $\mathcal{O}(sd^2 + d^3)$  FLOPs, while the latter requires at most  $\mathcal{O}(sdq)$  FLOPs<sup>4</sup>.

Each iteration of GIANT requires four rounds of communications: two one-to-all **Broadcast** of the full gradient  $\mathbf{g}_t \in \mathbb{R}^d$  or the model  $\mathbf{w}_t \in \mathbb{R}^d$  from the driver to all the workers and two all-to-one **Reduce** which aggregates the local directions to form  $\mathbf{g}_t$  or  $\tilde{\mathbf{p}}_t \in \mathbb{R}^d$ . If line search is used to determine the step size  $\beta_t$ , GIANT needs two extra rounds of communications: one **Broadcast** of  $\tilde{\mathbf{p}}_t$  and one **Reduce** that sums the local objective values. If the communication is in a tree fashion, the total per-iteration communication complexities is  $\mathcal{O}(d \log m)$  words.

### 1.3 Convergence Bounds

We study the convergence of  $\Delta_t \triangleq \mathbf{w}_t - \mathbf{w}^*$ , where  $\mathbf{w}_t$  is the output by the  $t$ -th iteration and  $\mathbf{w}^*$  is the unique optimal solution to (1). For quadratic loss, GIANT has global linear convergence which is almost independent of the condition number. (The condition number only affects the total number of iterations by an *additive logarithmic* term.) For general non-quadratic loss, such as logistic regression, GIANT has local linear-quadratic convergence.

To analyze the convergence, we assume that each local machine can access  $s$  ( $\gg d$ ) uniformly sampled feature vectors in order to compute a local Hessian matrix which approximates the true Hessian matrix. We let  $\epsilon \in (0, 1)$  be the error in approximating the Hessian matrix and  $\delta \in (0, 1)$  be the failure probability; the user can set  $\epsilon$  and  $\delta$  arbitrarily. (We denote the convergence tolerance by  $\mathcal{E}$ , not  $\epsilon$ .)

**Quadratic loss.** Given data points  $\{\mathbf{x}_i\}_{i=1}^n$ , denote the data matrix as

$$\mathbf{X} = \begin{bmatrix} - & \mathbf{x}_1^T & - \\ - & \mathbf{x}_2^T & - \\ & \vdots & \\ - & \mathbf{x}_n^T & - \end{bmatrix}_{n \times d}.$$

If the loss function of (1) is quadratic, e.g., linear regression, the Hessian matrix can simply be written as  $\mathbf{H} = \nabla^2 f(\mathbf{w}) = \frac{1}{n} \mathbf{X}^T \mathbf{X} + \mathbf{M}$ . Assume the local sample size is sufficiently big:

$$s = \Theta\left(\frac{\mu d}{\epsilon^2} \log \frac{dm}{\delta}\right),$$

where  $m$  is the number of partitions  $\mu \in [1, \frac{n}{d}]$  is the row coherence of the data matrix (see Section 2.1). Under this condition, the local Hessian matrices well approximate  $\mathbf{H}$  with

---

4. For the risk minimization problem, it is unnecessary to explicitly form the local Hessian matrices; we can efficiently compute a matrix  $\mathbf{A}_{t,i} \in \mathbb{R}^{s \times d}$  such that  $\tilde{\mathbf{H}}_{t,i} = \mathbf{A}_{t,i}^T \mathbf{A}_{t,i} + \mathbf{M}$ . Without explicitly forming the local Hessian matrices, the per-iteration complexity of CG is  $\mathcal{O}(sd)$ .

high probability (quantified by  $\epsilon$  and  $\delta$ ); as a consequence, GIANT is globally convergent:

$$\frac{\|\Delta_t\|_2}{\|\Delta_0\|_2} \leq \sqrt{\kappa} \cdot \left(\frac{\epsilon}{m} + \epsilon^2\right)^t \quad \text{holds with probability at least } 1 - \delta, \quad (2)$$

where  $\Delta_t \triangleq \mathbf{w}_t - \mathbf{w}^*$  and  $\kappa = \frac{\sigma_{\max}(\mathbf{H})}{\sigma_{\min}(\mathbf{H})}$  is the condition number of  $\mathbf{H}$ . If the coherence  $\mu$  is small, and the local sample size  $s$  is much larger than  $d$ , then  $\epsilon$  is small, and GIANT converges to high precision in very few iterations.<sup>5</sup> For fixed stopping criterion  $\|\Delta_t\|_2 \leq \mathcal{E}$ , the required number of iterations is

$$t = \frac{\log \frac{\|\Delta_0\|_2}{\mathcal{E}} + \frac{1}{2} \log \kappa}{\log \frac{1}{\epsilon/m + \epsilon^2}} = \Theta\left(\log \frac{1}{\mathcal{E}}\right) + \Theta(\log \kappa).$$

Importantly, GIANT achieves a *condition-number-independent* linear convergence rate, and the condition number only affects the total number of iterations by an *additive logarithmic* term. In contrast, DANE achieves a linear rate that has quadratic dependence on  $\kappa$ , while AIDE and DiSCO exhibit a square root dependence. This is very likely an artifact of their analysis, as DANE and AIDE are almost the same to GIANT for the quadratic case.

**General loss.** For general non-quadratic loss, we consider the local convergence behavior of GIANT, i.e., when the initialization,  $\mathbf{w}_0$ , is “close-enough” to the optimum,  $\mathbf{w}^*$ . Indeed, in general, global convergence of the Newton’s method is not guaranteed and one, typically, has to employ globalization techniques such as line-search and trust-region (Nocedal and Wright, 2006). Alternatively, one can consider a two-stage algorithm, where, initially, another globally-convergent distributed algorithm such as accelerated gradient descent is used to obtain an initial iterate  $\mathbf{w}_0$  for GIANT that is close enough to  $\mathbf{w}^*$ . We defer the global analysis of GIANT using various globalization methods for future work.

For the sequence of iterates,  $\mathbf{w}_0, \mathbf{w}_1, \dots, \mathbf{w}_t$ , generated by GIANT, let  $\mathbf{H}_0, \mathbf{H}_1, \dots, \mathbf{H}_t$  denote the corresponding Hessian matrices of the objective function,  $f$ . Assume that

$$\|\mathbf{H}_t - \mathbf{H}^*\|_2 \leq L \|\mathbf{w}_t - \mathbf{w}^*\|_2$$

for some finite  $L > 0$ . For the empirical risk minimization problem (1), the Hessian matrix can be written as  $\mathbf{H}_t = \mathbf{A}_t^T \mathbf{A}_t + \mathbf{M}$  for some  $\mathbf{A}_t \in \mathbb{R}^{n \times d}$ . Further assume the local sample size is sufficiently large:

$$s_t = \Theta\left(\frac{\mu_t d}{\epsilon^2} \log \frac{dm}{\delta}\right),$$

where  $\mu_t \in [1, \frac{n}{d}]$  is the row coherence of  $\mathbf{A}_t$ . Then it holds with probability at least  $1 - \delta$  that

$$\|\Delta_{t+1}\|_2 \leq \max \left\{ \left(\frac{\epsilon}{m} + \epsilon^2\right) \sqrt{\frac{\sigma_{\max}(\mathbf{H}_t)}{\sigma_{\min}(\mathbf{H}_t)}} \|\Delta_t\|_2, \frac{L}{\sigma_{\min}(\mathbf{H}_t)} \|\Delta_t\|_2^2 \right\}, \quad (3)$$

If we allow the sampling size  $s_t$  to increase as  $\mathbf{w}_t$  approaches  $\mathbf{w}^*$  such that the Hessian approximation error  $\epsilon \rightarrow 0$ , it follows that GIANT can achieve a locally *Q-superlinear*

---

5. If this assumption is violated, then fixed step size 1 is unsafe. We empirically observe that even if  $s$  is slightly smaller than  $d$ , where the assumption is obviously violated, GIANT with backtracking line search still converges rapidly. See Figure 5 for the empirical study.

convergence rate, i.e.,  $\limsup_t \|\Delta_{t+1}\|_2 / \|\Delta_t\|_2 = 0$ ; see [Roosta-Khorasani and Mahoney \(2016b\)](#). All prior distributed Newton-type methods do not have such local super-linear convergence guarantees. For  $m = 1$ , our result (3) is the same as the stochastic Newton-type methods studied in ([Roosta-Khorasani and Mahoney, 2016b](#), [Xu et al., 2016](#), [Pilanci and Wainwright, 2017](#)).

**Inexactly computing the local Newton directions.** In the above, we simply assume the local Newton directions are found by solving  $\tilde{\mathbf{H}}_{t,i}\mathbf{p} = \mathbf{g}_t$  “exactly” (e.g., by computing the matrix inverse in theory or iterating to machine precision in practice). To avoid this, we can let each worker *approximately* solve the linear system by taking roughly

$$q = \frac{\sqrt{\kappa_t}-1}{2} \log \frac{8}{\epsilon_0^2}$$

conjugate gradient (CG) steps initialized at zero. Here,  $\kappa_t$  is the condition number of  $\tilde{\mathbf{H}}_{t,i}$ , which is  $\epsilon$  close to that of  $\mathbf{H}_t$  w.p.  $1 - \delta$ , provided that  $s = \Theta\left(\frac{\mu t d}{\epsilon^2} \log \frac{m d}{\delta}\right)$ . The parameter  $\epsilon_0 \in (0, 1)$  is arbitrary and affects convergence. Using such inexact solutions, the bounds (2) and (3) with

$$\left(\frac{\epsilon}{m} + \epsilon^2\right) \quad \text{replaced by} \quad \epsilon_0 + \left(\frac{\epsilon}{m} + \epsilon^2\right)$$

hold with the same probability.

#### 1.4 Comparisons to Prior Works

GIANT bears a strong resemblance to DANE ([Shamir et al., 2014](#)) and AIDE ([Reddi et al., 2016](#)). In fact, if the loss function is quadratic, GIANT can be thought of as a special case of DANE and AIDE. However, in comparison, GIANT has some major advantages over the prior works DANE, AIDE, CoCoA ([Smith et al., 2016](#)), and DiSCO ([Zhang and Lin, 2015](#)).

- First and foremost, GIANT exhibits some more desirable convergence properties than the prior works. For *quadratic loss*, GIANT enjoys a fast global linear convergence rate which is *independent of the problem conditioning*. In contrast, DANE, AIDE, and DiSCO all have linear convergence rates which suffer from worse dependence on the condition number of the Hessian matrix, e.g., quadratic for DANE and square root dependence for AIDE and DiSCO. For *non-quadratic loss*, GIANT can achieve super-linear local convergence with more aggressive sampling, which has not been established for other methods.
- Second, GIANT is easy to implement and tune. More specifically, GIANT has one implicit parameter—the number of CG steps  $q$  taken by each worker to solve its local linear system.<sup>6</sup> In comparison, DANE has two parameters which appear explicitly in its formulation as well as at least two implicit parameters in its local solver—the number of iterations of a local solver and the learning rate. AIDE invokes DANE as its subroutine and, consequently, compared to DANE, has one more parameter in its

6. Although the backtracking line search has some parameters, their impact on the convergence is minimal in practice. Indeed the same parameters can be used for most problems without any need to fine-tuning. In contrast,  $q$  must be tuned to according to the condition number of the Hessian, which is problem-dependent and data-dependent.

formulation. Similarly, DiSCO and CoCoA has two explicit parameters as well as one implicit parameter—the number of iterations of a local solver.

- Third, our analysis makes explicit the impact of local sample size  $s$  and the coherence  $\mu$  of the data matrix, which do not appear in other similar works. More specifically, for both quadratic and non-quadratic losses, GIANT’s performance improves by increasing the local sample size  $s$ . This is quite intuitive as larger local sample size  $s$  results in more accurate local Hessian approximations. Among the prior works, only DANE’s theory (Shamir et al., 2014) for unregularized quadratic objective explicitly shows this property. Similarly, the role of matrix coherence  $\mu$ , which quantifies the heterogeneity in the data, has not been captured by previous similar theory. This is despite the fact that  $\mu$  can have a significant impact on the performance of distributed algorithms (Yang et al., 2016). For example, small  $\mu$  implies homogeneous samples, and thus a small subset of the samples might suffice to obtain a reasonable approximation to the full Hessian matrix, which in turn, yields fast convergence. This connection is not only established in our theory, but also clearly demonstrated in our experiments.

Our empirical studies of the  $\ell_2$ -regularized logistic regression show that in terms of both communication and local computation, GIANT, (inexact) DANE, and AIDE, have comparable performance, provided that the parameters of DANE and AIDE are fine tuned. Besides the iterations of the local solvers which is a common tuning parameter for all the three methods, we observe that the learning rate of the local solver of DANE and AIDE have very big influence upon their convergence. If we take into account the cost of tuning the learning rate, DANE and AIDE are much slower than GIANT.

Finally, we should emphasize that our proof techniques have little in common with the prior works DANE, AIDE, DiSCO, and CoCoA. Indeed, we employ a similar line of reasoning as (Pilanci and Wainwright, 2015, 2017, Roosta-Khorasani and Mahoney, 2016b, Xu et al., 2016). Our technical crux is the so-called subspace embedding property established by the randomized linear algebra community (Drineas et al., 2006a, Mahoney, 2011, Woodruff, 2014) and the improved subspace embedding made by model averaging (Wang et al., 2017). Such subspace embedding properties can be, probabilistically, established by using concentration bounds of positive semi-definite matrices (Tropp, 2015). Our theoretical analysis is easy to follow and extend.

## 2. Background

In this section, we give some preliminaries which can help with the clarity of exposition as well as self-containment of the present paper. More specifically, the notation used throughout this paper is introduced in Section 2.1 with commonly used notation summarized in Table 1. Section 2.2 briefly introduces matrix sketching. Section 2.3 gives a brief overview of Newton’s method in the context of problem formulation (1).

### 2.1 Notation

We now briefly introduce the notations used throughout this paper. The commonly used notation is summarized in Table 1.

Table 1: The commonly used notation.

Notation	Definition
$n$	number of samples
$m$	number of partitions
$s$	local samples size, may or may not equal to $\frac{n}{m}$
$\mathbf{x}_1, \dots, \mathbf{x}_n$	$d$ -dimensional feature vectors
$\mathbf{w}^* \in \mathbb{R}^d$	the optimal solution to (1)
$\mathbf{w}_t \in \mathbb{R}^d$	the output of the $t$ -th iteration
$f : \mathbb{R}^d \mapsto \mathbb{R}$	the objective function defined in (1)
$\mathbf{g}_t = \mathbf{g}(\mathbf{w}_t) \in \mathbb{R}^d$	the gradient of $f$ at $\mathbf{w}_t$
$\mathbf{H}_t = \mathbf{H}(\mathbf{w}_t) \in \mathbb{R}^{d \times d}$	the Hessian matrix of $f$ at $\mathbf{w}_t$
$\kappa_t$	the condition number of the Hessian matrix at $\mathbf{w}_t$
$\kappa$	the condition number of the Hessian matrix at $\mathbf{w}^*$
$\mathbf{A}_t \in \mathbb{R}^{n \times d}$	the matrix that satisfies $\mathbf{A}_t^T \mathbf{A}_t + \mathbf{M} = \mathbf{H}_t$
$\mu_t$ or $\mu$	the row coherence of $\mathbf{A}_t$

**Matrices and vectors.** Matrices and vectors are, respectively, denoted by bold upper-case and bold lower-case letters. We take  $\mathbf{I}_n$  to be the  $n \times n$  identity matrix,  $\mathbf{0}$  to be a vector or matrix of all zeroes of the appropriate size, and  $\mathbf{1}_n$  to be the  $n$ -dimensional vector of all ones. Subscripts denote iteration counter, e.g.,  $\mathbf{A}_t$  and  $\mathbf{b}_t$  denote, respectively, the matrix and vector arising in iteration  $t$ .

**Sets.** The set  $\{1, 2, \dots, n\}$  is denoted by  $[n]$ . We call  $\{\mathcal{J}_1, \dots, \mathcal{J}_k\}$  a  $k$ -partition of  $[n]$  if  $\mathcal{J}_1 \cup \dots \cup \mathcal{J}_k = [n]$  and  $\mathcal{J}_p \cap \mathcal{J}_q = \emptyset$  when  $p \neq q$ . Cardinality of the set  $\mathcal{J}$  is denoted by  $|\mathcal{J}|$ .

**Singular value decomposition (SVD).** Let  $\mathbf{A} \in \mathbb{R}^{n \times d}$  and  $\rho = \text{rank}(\mathbf{A})$ . A (compact) singular value decomposition (SVD) is defined by

$$\mathbf{A} = \mathbf{U}\mathbf{\Sigma}\mathbf{V}^T = \sum_{i=1}^{\rho} \sigma_i \mathbf{u}_i \mathbf{v}_i^T,$$

where  $\mathbf{U}$ ,  $\mathbf{\Sigma}$ ,  $\mathbf{V}$  are a  $n \times \rho$  column-orthogonal matrix, a  $\rho \times \rho$  diagonal matrix with nonnegative entries, and a  $d \times \rho$  column-orthogonal matrix, respectively. If  $\mathbf{A}$  is symmetric positive semi-definite (SPSD), then  $\mathbf{U} = \mathbf{V}$ , and this decomposition is, at times, referred to as the (reduced) eigenvalue decomposition (EVD). By convention, singular values are ordered such that  $\sigma_1 \geq \dots \geq \sigma_\rho$ .

**Leverage score and coherence.** Let  $\mathbf{U} \in \mathbb{R}^{n \times \rho}$  be defined in the above and  $\mathbf{u}_i$  be the  $i$ -th row of  $\mathbf{U}$ . The row leverage scores of  $\mathbf{A}$  are  $\|\mathbf{u}_i\|_2^2$  for  $i \in [n]$ . The row coherence of  $\mathbf{A}$  is  $\mu(\mathbf{A}) = \frac{n}{\rho} \max_i \|\mathbf{u}_i\|_2^2$ . See [Drineas et al. \(2012\)](#) for more details.

**Matrix norms.** The following matrix norms are used throughout this paper:

$$\begin{aligned} \text{Frobenius Norm: } \quad & \|\mathbf{A}\|_F = \sqrt{\sum_{i,j} a_{ij}^2} = \sqrt{\sum_i \sigma_i^2(\mathbf{A})}; \\ \text{Spectral Norm: } \quad & \|\mathbf{A}\|_2 = \max_{\|\mathbf{x}\|_2=1} \|\mathbf{A}\mathbf{x}\|_2 = \sigma_1(\mathbf{A}). \end{aligned}$$

## 2.2 Matrix Sketching

Here, we briefly review matrix sketching methods that are commonly used for randomized linear algebra (RLA) applications (Mahoney, 2011). Given a matrix  $\mathbf{A} \in \mathbb{R}^{n \times d}$ , we refer to  $\mathbf{C} = \mathbf{S}^T \mathbf{A} \in \mathbb{R}^{s \times d}$  as *sketch* of  $\mathbf{A}$  with the *sketching matrix*  $\mathbf{S} \in \mathbb{R}^{n \times s}$  (typically  $s \ll n$ ). In many RLA applications, the rows of  $\mathbf{C}$  are typically made up of a randomly selected and rescaled subset of the rows of  $\mathbf{A}$ , or their random linear combinations; the former type of sketching is called *row selection* or *random sampling*, and the latter is referred to as *random projection*. Such randomized sketching has emerged as a powerful primitive in RLA for dealing with large-scale matrix computation problems (Mahoney, 2011, Drineas and Mahoney, 2016). This is mainly due to the fact that sketching, if done right, allows for large matrices to be “represented” by smaller alternatives which are more amenable to efficient computations and storage, while provably retaining certain desired properties of the original matrices (Mahoney, 2011, Woodruff, 2014).

Here, we consider matrix multiplication formulation of *row selection* in which the sketched matrix,  $\mathbf{C} \in \mathbb{R}^{s \times d}$ , is constructed using a randomly sampled and particularly rescaled subset of the rows of  $\mathbf{A} \in \mathbb{R}^{n \times d}$ . More specifically, let  $p_1, \dots, p_n \in (0, 1)$  be the sampling probabilities associated with the rows of  $\mathbf{A}$  (so that, in particular,  $\sum_{i=1}^n p_i = 1$ ). The rows of the sketch are selected independently and according to the sampling distribution  $\{p_i\}_{i=1}^n$  such that we have

$$\mathbb{P}(\mathbf{c}_i = \mathbf{a}_j / \sqrt{sp_j}) = p_j, \quad \text{for all } j = 1, 2, \dots, n,$$

where  $\mathbf{c}_i$  and  $\mathbf{a}_j$  are  $i^{\text{th}}$  and  $j^{\text{th}}$  rows of  $\mathbf{C}$  and  $\mathbf{A}$ , respectively. As a result, the sketching matrix  $\mathbf{S} \in \mathbb{R}^{n \times s}$  contains exactly one non-zero entry in each column, whose position and magnitude correspond to the selected row of  $\mathbf{A}$ . *Uniform sampling* is a particular form of row sampling with  $p_1 = \dots = p_n = 1/n$ , while *leverage score sampling* takes  $p_i$  proportional to the  $i$ -th leverage score of  $\mathbf{A}$  for  $i \in [n]$  (or its randomized approximation (Drineas et al., 2012)).

*Random projection* forms a sketch by taking random linear combinations of the rows of  $\mathbf{A}$ . Popular random projections include, among many others, Gaussian projection (Johnson and Lindenstrauss, 1984), subsampled randomized Hadamard transform (Drineas et al., 2011, Lu et al., 2013, Tropp, 2011), Rademacher random variables (Achlioptas, 2003), CountSketch (Clarkson and Woodruff, 2013, Meng and Mahoney, 2013, Nelson and Nguyễn, 2013).

## 2.3 Newton’s Method

We now briefly review classical Newton’s method in the context of the empirical risk minimization problem (1) considered in this paper. Given any iterate  $\mathbf{w}_t$ , let the gradient and Hessian matrix of  $f : \mathbb{R}^d \mapsto \mathbb{R}$  at  $\mathbf{w}_t$  in (1) be, respectively, written as

$$\mathbf{g}_t = \mathbf{g}(\mathbf{w}_t) = \nabla f(\mathbf{w}_t) = \frac{1}{n} \sum_{i=1}^n l'_i(\mathbf{w}_t^T \mathbf{x}_i) \mathbf{x}_i + \mathbf{M} \mathbf{w}_t = \mathbf{A}_t^T \mathbf{b}_t + \mathbf{M} \mathbf{w}_t, \quad (4)$$

$$\mathbf{H}_t = \mathbf{H}(\mathbf{w}_t) = \nabla^2 f(\mathbf{w}_t) = \frac{1}{n} \sum_{i=1}^n l''_i(\mathbf{w}_t^T \mathbf{x}_i) \mathbf{x}_i \mathbf{x}_i^T + \mathbf{M} = \mathbf{A}_t^T \mathbf{A}_t + \mathbf{M}, \quad (5)$$

where

$$\mathbf{A}_t = \frac{1}{\sqrt{n}} \left[ \sqrt{l_1''(\mathbf{w}_t^T \mathbf{x}_1)} \mathbf{x}_1, \dots, \sqrt{l_n''(\mathbf{w}_t^T \mathbf{x}_n)} \mathbf{x}_n \right]^T \in \mathbb{R}^{n \times d}, \quad (6)$$

$$\mathbf{b}_t = \frac{1}{\sqrt{n}} \left[ \frac{l_1'(\mathbf{w}_t^T \mathbf{x}_1)}{\sqrt{l_1''(\mathbf{w}_t^T \mathbf{x}_1)}}, \dots, \frac{l_n'(\mathbf{w}_t^T \mathbf{x}_n)}{\sqrt{l_n''(\mathbf{w}_t^T \mathbf{x}_n)}} \right]^T \in \mathbb{R}^n, \quad (7)$$

with  $l_i'$  and  $l_i''$  being, respectively, the first and second order derivatives of  $l_i : \mathbb{R} \mapsto \mathbb{R}$ . Iterations of the classical Newton's method is of the form  $\mathbf{w}_{t+1} = \mathbf{w}_t - \mathbf{p}_t^*$ , where

$$\mathbf{p}_t^* = \mathbf{H}_t^{-1} \mathbf{g}_t = (\mathbf{A}_t^T \mathbf{A}_t + \mathbf{M})^{-1} (\mathbf{A}_t^T \mathbf{b}_t + \mathbf{M} \mathbf{w}_t). \quad (8)$$

is the Newton's direction. Explicit examples of  $\mathbf{A}_t$  and  $\mathbf{b}_t$  for linear and logistic regressions are given in Appendix A.

Newton's method is well known to enjoy locally quadratic convergence, i.e., in a certain neighborhood around the solution  $\mathbf{w}^*$ , as iterations progress, the number of accurate digits of  $\mathbf{w}_t$  doubles per iteration (of course assuming a setting with infinite precision). However, globally the behavior of *pure* Newton's might not be as stellar. For example, simple examples have been constructed for which pure Newton's method, when initialized outside its local basin of attraction, fails to converge (Polyak, 2007). In this light, there are various *globalization* techniques which aim at modifications of pure Newton's method to achieve global convergence, e.g., line search, trust-region (Nocedal and Wright, 2006). In this paper, we employ backtracking line search, which modifies the iteration of the pure Newton's method as  $\mathbf{w}_{t+1} = \mathbf{w}_t - \beta_t \mathbf{p}_t^*$ , for some appropriate step size  $\beta_t \in (0, 1]$ . Such modifications of Newton's method, in the context of Hessian approximation, has shown to be globally convergent (Roosta-Khorasani and Mahoney, 2016a).

Finally, although here we only consider convex settings, Newton-type methods using inexact Hessian information have been recently studied in the context of non-convex applications, e.g., Roosta-Khorasani et al. (2014a,b, 2015), Roosta-Khorasani (2015), Xu et al. (2017a,b). We leave the study of the distributed variants of these Newton-type methods for non-convex problems for future research.

### 3. Our Main GIANT Algorithm

We are now ready to present our main algorithm, GIANT. To do so, in Section 3.1, we first discuss the data-partitioning considered in this paper. The details of our algorithm are then described in Section 3.2. In particular, GIANT is summarized in Algorithm 1 with conceptual illustrations in Figure 1. This is then followed by some discussions on solutions to the GIANT's sub-problems and other practical issues, respectively, in Sections 3.3 and 3.4.

#### 3.1 Data Partitioning

Suppose the  $n$  feature vectors and loss functions  $(\mathbf{x}_1, l_1), \dots, (\mathbf{x}_n, l_n)$  are partitioned among  $m$  worker machines. Let  $s \triangleq \frac{n}{m}$  be the local sample size. ( $s$  can be different from  $\frac{n}{m}$ ; we discuss this in the subsequent paragraph.) Let  $\mathbf{A}_t \in \mathbb{R}^{n \times d}$  and  $\mathbf{b}_t \in \mathbb{R}^n$  be defined in (6) and (7), respective. Let  $\mathbf{A}_{t,1}, \dots, \mathbf{A}_{t,m} \in \mathbb{R}^{s \times d}$  and  $\mathbf{b}_{t,1}, \dots, \mathbf{b}_{t,m} \in \mathbb{R}^s$  be the corresponding

partition of  $\mathbf{A}_t$  and  $\mathbf{b}_t$ . GIANT uses  $(\mathbf{A}_{t,i}, \mathbf{b}_{t,i})$  to compute the local gradient  $\mathbf{g}_{t,i}$  and uses  $\mathbf{A}_{t,i}$  to compute the local approximate Newton direction  $\tilde{\mathbf{p}}_{t,i}$ .

This disjoint partition has one limitation: to make the local sample size,  $s$ , big compared to  $d$ , one cannot use too many worker machine (otherwise each partition is over-small), which limits the level of parallelism and scalability. One solution is making the partition have *overlap*, that is, copies of one sample can be held by multiple machines. In this way, *the local sample size  $s$  can be much larger than  $\frac{n}{m}$* ; even if the number of partitions,  $m$ , is very large,  $s$  can still be big compared to  $d$ , making the Hessian matrix approximation reasonably well. Our convergence bounds directly apply to both kinds of partition.

### 3.2 Algorithm Description

In the  $t$ -th iteration, the  $i$ -th worker computes  $\mathbf{A}_{t,i} \in \mathbb{R}^{s \times d}$  and  $\mathbf{b}_{t,i} \in \mathbb{R}^{\frac{n}{m}}$ ; the local Hessian matrix is  $\tilde{\mathbf{H}}_{t,i} = \frac{n}{s} \mathbf{A}_{t,i}^T \mathbf{A}_{t,i} + \mathbf{M}$ ; the local gradient is  $\mathbf{g}_{t,i} = \mathbf{A}_{t,i}^T \mathbf{b}_{t,i}$ . The full gradient can then be obtained by aggregating local gradients as

$$\mathbf{g}_t = \mathbf{M}\mathbf{w}_t + \mathbf{A}_t^T \mathbf{b}_t = \mathbf{M}\mathbf{w}_t + \sum_{i=1}^m \mathbf{g}_{t,i},$$

which can be computed by one Reduce operation and will be Broadcast to all the workers. The local Approximate NewTon (ANT) direction (in the  $t$ -th iteration, of the  $i$ -th worker)  $\tilde{\mathbf{p}}_{t,i}$  is obtained by (approximately) solving the linear system

$$\tilde{\mathbf{H}}_{t,i} \mathbf{p} = \mathbf{g}_t, \quad \text{equivalently,} \quad \left( \frac{n}{s} \mathbf{A}_{t,i}^T \mathbf{A}_{t,i} + \mathbf{M} \right) \mathbf{p} = \mathbf{g}_t. \quad (9)$$

Finally, the driver combines the ANT directions to get a Globally Improved ANT (GIANT) direction  $\tilde{\mathbf{p}}_t = \frac{1}{m} \sum_{i=1}^m \tilde{\mathbf{p}}_{t,i}$  (which also requires one Reduce operation), performs the update  $\mathbf{w}_{t+1} = \mathbf{w}_t - \tilde{\mathbf{p}}_t$ , and Broadcast  $\mathbf{w}_{t+1}$  to all the workers. Therefore, each iteration performs two Reduce and two Broadcast operations. The above iterations can be summarized as

$$\begin{aligned} \mathbf{w}_{t+1} &= \mathbf{w}_t - \frac{1}{m} \sum_{i=1}^m \tilde{\mathbf{p}}_{t,i} \\ &= \mathbf{w}_t - \frac{1}{m} \sum_{i=1}^m \tilde{\mathbf{H}}_{t,i}^{-1} \mathbf{g}_t \\ &= \mathbf{w}_t - \frac{1}{m} \sum_{i=1}^m \tilde{\mathbf{H}}_{t,i}^{-1} \left[ \mathbf{M}\mathbf{w}_t + \sum_{i=1}^m \mathbf{g}_{t,i} \right] \end{aligned}$$

where  $\tilde{\mathbf{H}}_{t,i}$  and  $\mathbf{g}_{t,i}$  are computed locally and each summation is performed by one Reduce operation. Algorithm 1 gives the steps of GIANT, while the schematic of an iteration is depicted in Figure 1.

**Line search.** After computing a Newton direction  $\tilde{\mathbf{p}}_t$ , the update is then given by  $\mathbf{w}_{t+1} = \mathbf{w}_t - \beta_t \tilde{\mathbf{p}}_t$ , for suitably chosen step size  $\beta_t$ . Under certain assumptions (e.g., vicinity to  $\mathbf{w}^*$ ), Algorithm 1 with the fixed step size  $\beta_t = 1$  is safe and convergence is guaranteed. Under two circumstances, line search strategy should be used to find an appropriate  $\beta_t$ . First, for non-quadratic loss, and starting from an arbitrary  $\mathbf{w}_0$  (not necessarily close to  $\mathbf{w}^*$ ), line

---

**Algorithm 1** Globally Improved Approximate Newton (GIANT).

---

- 1: **Input:** the  $n$  data samples randomly partitioned among  $m$  workers; a single-machine program for solving linear equations, e.g., CG.
  - 2: Optional: if  $\frac{n}{m}$  is much smaller than the number of features,  $d$ , make copies of every sample and shuffle the data; in this way, the local sample size  $s$  is bigger than  $d$ ;
  - 3: Optional: the  $i$ -th worker solves (1) using the local data and get  $\mathbf{w}_{0,i}$ , for all  $i \in [m]$ ; then the driver compute  $\mathbf{w}_0 = \frac{1}{m} \sum_{i=1}^m \mathbf{w}_{0,i}$ ;
  - 4: **for**  $t = 0, 1, 2, \dots$  **do**
  - 5:   **Broadcast**  $\mathbf{w}_t$  to all the workers;
  - 6:   In parallel, the  $i$ -th worker locally computes  $\mathbf{A}_{t,i}$  and  $\mathbf{b}_{t,i}$  according to Section 3.1;
  - 7:   In parallel, the  $i$ -th worker locally computes  $\mathbf{g}_{t,i} = \mathbf{A}_{t,i}^T \mathbf{b}_{t,i}$ ;
  - 8:   The driver computes the gradient  $\mathbf{g}_t = \mathbf{M}\mathbf{w}_t + \sum_{i=1}^m \mathbf{g}_{t,i}$  by Reduce;
  - 9:   **Broadcast**  $\mathbf{g}_t$  to all the workers;
  - 10:   In parallel, the  $i$ -th worker locally compute ANT direction  $\tilde{\mathbf{p}}_{t,i}$  by solving  $(\frac{n}{s} \mathbf{A}_{t,i}^T \mathbf{A}_{t,i} + \mathbf{M})\mathbf{p} = \mathbf{g}_t$ ;
  - 11:   The driver computes GIANT direction  $\tilde{\mathbf{p}}_t = \frac{1}{m} \sum_{i=1}^m \tilde{\mathbf{p}}_{t,i}$  by Reduce;
  - 12:   The driver performs update  $\mathbf{w}_{t+1} = \mathbf{w}_t - \beta_t \tilde{\mathbf{p}}_t$ , where  $\beta_t$  can be fixed as one or determined by line search;
  - 13: **end for**
  - 14: **return**  $\mathbf{w}_{t+1}$ .
- 

search must be applied to guarantee global convergence. Second, when the local sample size,  $s$ , is not sufficiently larger than  $d$ , the Hessian approximation is very rough and our theory does not apply at all; even if  $s$  is slightly smaller than  $d$ , in practice, GIANT with line search still has rapid convergence, but GIANT with the fixed step size  $\beta_t = 1$  diverges (see Figure 5).

We can slightly modify Algorithm 1 to enable line search at the cost of two additional rounds of communications per iteration, one for aggregating vectors of constant dimension into one by Reduce and the other for **Broadcasting** a scalar. After Step 11 of Algorithm 1, the driver **Broadcast**  $\tilde{\mathbf{p}}_t$ . Then the  $i$ -th worker computes the local objective values

$$\frac{1}{n} \sum_{j \in \mathcal{J}_i} f_j(\mathbf{w}_t - \beta \tilde{\mathbf{p}}_t)$$

for all  $\beta$  in the set  $\mathcal{B}$ ; we fix  $\mathcal{B} = \{4^0, 4^{-1}, \dots, 4^{-9}\}$  throughout our experiments. With an Reduce operation, the driver holds the set  $\{f(\mathbf{w}_t - \beta \tilde{\mathbf{p}}_t)\}_{\beta \in \mathcal{B}}$ , picks  $\beta_t$  using backtracking line search, and performs a **Broadcast**  $\beta_t$  such that the driver and workers can then locally perform the update  $\mathbf{w}_{t+1} = \mathbf{w}_t - \beta_t \tilde{\mathbf{p}}_t$ . Throughout, we fix the control parameter of backtracking line search to  $c = 0.1$ . In practice, there is little point in tuning the parameters of line search; the parameters  $\mathcal{B}$  and  $c$  can be fixed for whatever objective function and whatever data.

### 3.3 Exact versus Inexact Local Newton Directions

In the  $t$ -th iteration of GIANT, each worker solves the local problem (9), either exactly by inverting the local Hessian matrix  $\tilde{\mathbf{H}}_{t,i} \in \mathbb{R}^{d \times d}$  or inexactly by employing an iterative solver such as CG. The computational costs of these two approaches can be obtained as follows.

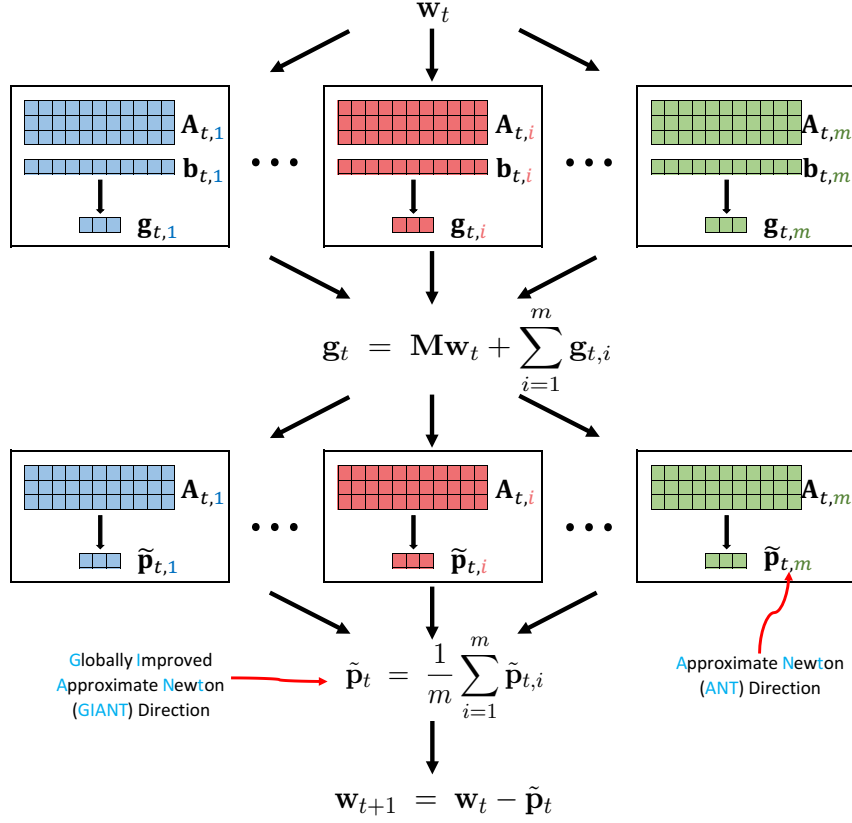


Figure 1: One iteration of GIANT.

- Exact solution. The formation of a local Hessian matrix  $\tilde{\mathbf{H}}_{t,i} \in \mathbb{R}^{d \times d}$  costs  $\mathcal{O}(sd^2)$  FLOPs; the inversion of  $\tilde{\mathbf{H}}_{t,i}$  costs  $\mathcal{O}(d^3)$  FLOPs. For quadratic loss, the local Hessian matrices do not change with  $t$ , and thus such computations are performed only once, whereas for nonquadratic loss, such computations have to be performed in each iteration.

- Inexact solution. We can equivalently find a local Newton direction by minimizing

$$\|\tilde{\mathbf{H}}_{t,i}\mathbf{p} - \mathbf{g}_t\|_2^2 = \left\| \begin{pmatrix} n \\ s \end{pmatrix} \mathbf{A}_{t,i}^T \mathbf{A}_{t,i} + \mathbf{M} \right) \mathbf{p} - \mathbf{g}_t \right\|_2^2$$

using  $q = \mathcal{O}(\sqrt{\kappa_t})$  steps of CG, which costs  $\mathcal{O}(sdq) = \mathcal{O}(sd\sqrt{\kappa_t})$  FLOPs.

Based on the above costs, one can make the following observations. Let  $T$  be the maximum iterations of GIANT.

- For quadratic loss, if  $d = \mathcal{O}(T\sqrt{\kappa})$ , it is worthwhile to form and invert the local Hessian matrices; each worker spends in total  $\mathcal{O}(sd^2 + d^3 + Tsd)$  FLOPs. Otherwise, if  $d = \Omega(T\sqrt{\kappa})$ , inexact solution by CG without forming the local Hessian matrices is preferable; each worker spends in total  $\mathcal{O}(Tsd\sqrt{\kappa})$  FLOPs.

- For nonquadratic loss, inexact solution by CG is usually preferable. In this case, each worker spends in total  $\mathcal{O}(Tsd\sqrt{\kappa})$  FLOPs. In contrast, using exact solutions, each worker would require  $\mathcal{O}(Tsd^2)$  FLOPs.<sup>7</sup>

Besides, if  $\mathbf{X}$  is sparse,  $\mathbf{A}_t$  is also sparse, but  $\tilde{\mathbf{H}}_{t,i}$  is dense. As sparse matrix-vector product is cheap, iteratively solving  $(\frac{n}{s}\mathbf{A}_{t,i}^T\mathbf{A}_{t,i} + \mathbf{M})\mathbf{p} = \mathbf{g}_t$  by CG is cheaper than computing  $\tilde{\mathbf{H}}_{t,i}^{-1}\mathbf{g}_t$ .

### 3.4 Other Practical Considerations

**Initialization.** GIANT can be initialized using an arbitrary starting point. In practice, model averaging (Zhang et al., 2013, Wang et al., 2017) can often produce an initialization in the vicinity of the optimal solution. Model averaging typically amounts to each worker solving a subproblem using its local data, followed by averaging the local solutions, e.g., Zhang et al. (2013) analyzed the averaged solution for general problems; Wang et al. (2017) established a strong error bound for the ridge regression problem.

**Avoiding straggler problem.** Figure 1 shows that GIANT follows the bulk synchronous parallel communication model (Valiant, 1990). In each iteration, due to various reasons (e.g., software or hardware failures, etc), a few nodes can be slower than the rest and thereby significantly slow down the overall execution. Such nodes are called stragglers. For GIANT, the computation of the full gradient  $\mathbf{g}_t$  requires only several matrix-vector multiplications and thus unlikely to cause severe straggler problem; however, employing an iterative linear system solver such as CG to obtain the local approximate Newton directions  $\tilde{\mathbf{p}}_{t,1}, \dots, \tilde{\mathbf{p}}_{t,m}$ , can result in some degree of straggler problem. Fortunately, GIANT can naturally remedy this issue. More specifically, in Figure 1, instead of computing  $\tilde{\mathbf{p}}_t = \frac{1}{m} \sum_{i=1}^m \tilde{\mathbf{p}}_{t,i}$ , one can set  $m' < m$ , e.g.,  $m' = \lceil 0.5m \rceil$ , let  $\tilde{\mathbf{p}}_t$  be the average of the  $m'$  earliest returned local approximate Newton directions, and ignore the rest of the  $m - m'$  nodes in this iteration. This way, if we replace  $m$  by  $m'$ , Theorems 1, 2, 4, and Corollary 3 continue to hold.

## 4. Convergence Analysis

In this section we present the details of the convergence analysis of GIANT. Section 4.1 focuses on quadratic loss and treats the global convergence of GIANT. We then expand to non-quadratic loss and describe the local convergence properties of GIANT in Section 4.2. For the results of Sections 4.1 and 4.2, we require that the local linear system to obtain the local Newton direction is solved exactly. Section 4.3 then relaxes this requirement to allow for inexactness in local Newton directions, and establishes similar convergence rates as those of exact variants. In Section 4.4, we then discuss the impacts of local sample size  $s$ , number of partitions  $m$ , condition number  $\kappa$ , matrix coherence  $\mu$ , and some other factors. In Section 4.5 we outline the proofs of convergence bounds.

---

7. In the non-quadratic case, note that in the local region,  $\kappa_t = \Theta(\kappa)$  where  $\kappa$  is the condition number of  $\mathbf{H}(\mathbf{w}^*)$ .

## 4.1 Quadratic Loss

Let  $\mathbf{M} \in \mathbb{R}^{d \times d}$  be any SPSD matrix. We consider the quadratic optimization problems:

$$f(\mathbf{w}) = \frac{1}{2n} \|\mathbf{X}\mathbf{w} - \mathbf{y}\|_2^2 + \frac{1}{2} \mathbf{w}^T \mathbf{M} \mathbf{w}, \quad (10)$$

which is a special case of (1) where  $l_i(z) = \frac{1}{2}(z - y_i)^2$ . The Hessian matrix is given as  $\nabla^2 f(\mathbf{w}) = \frac{1}{n} \mathbf{X}^T \mathbf{X} + \mathbf{M}$ , which does not depend on  $\mathbf{w}$ . Theorem 1 describes the convergence of  $\Delta_t \triangleq \mathbf{w}_t - \mathbf{w}^*$ , where  $\mathbf{w}^*$  is the solution to (10).

**Theorem 1** *Let  $\mu \in [1, \frac{n}{d}]$  be the row coherence of  $\mathbf{X} \in \mathbb{R}^{n \times d}$ ,  $m$  be the number of partitions, and  $\epsilon, \delta \in (0, 1)$  be fixed error parameters. Assume the local sample size satisfies  $s = \Theta(\frac{\mu d}{\epsilon^2} \log \frac{md}{\delta})$ . It holds with probability  $1 - \delta$  that*

$$\frac{\|\Delta_t\|_2}{\|\Delta_0\|_2} \leq \alpha^t \sqrt{\kappa}, \quad (11)$$

where  $\alpha = \vartheta(\frac{\epsilon}{m} + \epsilon^2)$ ,  $\vartheta = \frac{\sigma_{\max}^2(\mathbf{X})}{\sigma_{\max}^2(\mathbf{X}) + \sigma_{\min}(\mathbf{M})} \leq 1$ , and  $\kappa$  is the condition number of  $\mathbf{H} = \frac{1}{n} \mathbf{X}^T \mathbf{X} + \mathbf{M}$ .

The role of matrix coherence  $\mu$  and the sample size  $s$  can be easily observed from Theorem 1. More specifically, if  $\mathbf{X}$ 's coherence,  $\mu$ , is small and  $s$  is large enough compared to  $d$ , then we obtain a linear convergence rate in the error,  $\|\Delta_t\|_2$ .

## 4.2 General Smooth Loss

For non-quadratic but smooth loss, GIANT has linear-quadratic local convergence, which is formally stated in Theorem 2 and Corollary 3. In the non-quadratic case, we make the following standard assumption about the local regularity of the Hessian of  $f$  at the optimum,  $\mathbf{w}^*$ .

**Assumption 1** *The Hessian matrix is  $L$ -Lipschitz at  $\mathbf{w}^*$ :  $\|\mathbf{H}(\mathbf{w}_t) - \mathbf{H}(\mathbf{w}^*)\|_2 \leq L \|\mathbf{w}_t - \mathbf{w}^*\|_2$ .*

Theorem 2 establishes the local linear-quadratic convergence of  $\Delta_t \triangleq \mathbf{w}_t - \mathbf{w}^*$ . Here we let  $\mathbf{A}_t \in \mathbb{R}^{n \times d}$  be defined in (6) (thus  $\mathbf{A}_t^T \mathbf{A}_t + \mathbf{M} = \mathbf{H}_t$ ). Note that the coherence of  $\mathbf{A}_t$ , denote  $\mu_t$ , changes with iteration.

**Theorem 2** *Let  $\mu_t \in [1, \frac{n}{d}]$  be the coherence of  $\mathbf{A}_t$  and  $\epsilon, \delta \in (0, 1)$  be fixed error parameters, and  $m$  be the number of partitions. Assume the local sample size satisfies  $s_t = \Theta(\frac{\mu_t d}{\epsilon^2} \log \frac{md}{\delta})$ . Under Assumption 1, it holds with probability  $1 - \delta$  that*

$$\|\Delta_{t+1}\|_2 \leq \max \left\{ \alpha \sqrt{\frac{\sigma_{\max}(\mathbf{H}_t)}{\sigma_{\min}(\mathbf{H}_t)}} \|\Delta_t\|_2, \frac{2L}{\sigma_{\min}(\mathbf{H}_t)} \|\Delta_t\|_2^2 \right\},$$

where  $\alpha = \vartheta(\frac{\epsilon}{m} + \epsilon^2)$  and  $\vartheta = \frac{\sigma_{\max}^2(\mathbf{A}_t)}{\sigma_{\max}^2(\mathbf{A}_t) + \sigma_{\min}(\mathbf{M})} \leq 1$ .

Note that in Theorem 2 the convergence depends on the condition numbers of the Hessian at every point, i.e., it is iteration dependent via  $\mathbf{H}_t$ . Due to the Lipschitz assumption on the Hessian, it is easy to see that the condition number of the Hessian in a neighborhood of  $\mathbf{w}^*$  is close to  $\kappa(\mathbf{H}^*)$ . This simple observation implies Corollary 3, in which the dependence of the local convergence of GIANT on iterations via  $\mathbf{H}_t$  is removed. For this, we need to make the following assumption which describes a neighborhood radius around  $\mathbf{w}^*$ , in which such local iteration independent local convergence is obtained. (Although  $\vartheta$  depends on  $\mathbf{H}_t$ ,  $\vartheta$  can be removed because  $\vartheta \leq 1$ .)

**Assumption 2** Assume  $\mathbf{w}_t$  is close to  $\mathbf{w}^*$  in that  $\|\Delta_t\|_2 \leq \frac{\sigma_{\min}(\mathbf{H}^*)}{3L}$ , where  $L$  is defined in Assumption 1.

**Corollary 3** Let the notation be defined in Theorem 2. Under Assumptions 1 and 2, it holds with probability  $1 - \delta$  that

$$\|\Delta_{t+1}\|_2 \leq \max \left\{ 2\alpha \sqrt{\frac{\sigma_{\max}(\mathbf{H}^*)}{\sigma_{\min}(\mathbf{H}^*)}} \|\Delta_t\|_2, \frac{3L}{\sigma_{\min}(\mathbf{H}^*)} \|\Delta_t\|_2^2 \right\}.$$

### 4.3 Inexact Solutions to Local Quadratic Sub-Problems

In the  $t$ -th iteration, the  $i$ -th worker locally computes  $\tilde{\mathbf{p}}_{t,i}$  by solving  $\tilde{\mathbf{H}}_{t,i} \mathbf{p} = \mathbf{g}_t$ , where  $\tilde{\mathbf{H}}_{t,i} = \frac{n}{s} \mathbf{A}_{t,i}^T \mathbf{A}_{t,i} + \mathbf{M}$  is the  $i$ -th local Hessian matrix. When the order of magnitude of  $d$  is higher than  $10^4$ , the exact formation of  $\tilde{\mathbf{H}}_{t,i} \in \mathbb{R}^{d \times d}$  and its inversion are impractical, so we employ iterative linear system solvers, such as CG, to inexactly solve the arising linear system. Let  $\tilde{\mathbf{p}}'_{t,i}$  be an inexact solution which is close to  $\tilde{\mathbf{p}}_{t,i} \triangleq \tilde{\mathbf{H}}_{t,i}^{-1} \mathbf{g}_t$ , in the sense that

$$\left\| \tilde{\mathbf{H}}_{t,i}^{1/2} (\tilde{\mathbf{p}}'_{t,i} - \tilde{\mathbf{p}}_{t,i}) \right\|_2 \leq \frac{\epsilon_0}{2} \left\| \tilde{\mathbf{H}}_{t,i}^{1/2} \tilde{\mathbf{p}}_{t,i} \right\|_2, \quad (12)$$

for some  $\epsilon_0 \in (0, 1)$ . GIANT then takes  $\tilde{\mathbf{p}}'_t = \frac{1}{m} \sum_{i=1}^m \tilde{\mathbf{p}}'_{t,i}$  as the approximate Newton direction in lieu of  $\tilde{\mathbf{p}}_t$ . In this case, as long as  $\epsilon_0$  is of the same order as  $\frac{\epsilon}{m} + \epsilon^2$ , the convergence rate of such inexact variant of GIANT remains similar to the case that the local linear system is solved exactly. Theorem 4 and Corollary 5 give convergence properties of inexact GIANT.

**Theorem 4** In Algorithm 1, we replace  $\tilde{\mathbf{p}}_{t,i}$  by the inexact local solution  $\tilde{\mathbf{p}}'_{t,i}$ . Assume (12) holds. Then Theorems 1 and 2 and Corollary 3, with

$$\alpha = \vartheta \left( \frac{\epsilon}{m} + \epsilon^2 \right) \quad \text{replaced by} \quad \alpha' = \vartheta \left( \frac{\epsilon}{m} + \epsilon^2 \right) + \epsilon_0,$$

all hold with the same probability.

**Corollary 5** To compute an inexact local Newton direction, in each iteration, each worker uses all-zero initialization of  $\mathbf{p}$  and optimizes  $\|\tilde{\mathbf{H}}_{t,i} \mathbf{p} - \mathbf{g}_t\|_2^2$  by taking

$$q = \log \frac{8}{\epsilon_0^2} / \log \frac{\sqrt{\tilde{\kappa}_t} + 1}{\sqrt{\tilde{\kappa}_t} - 1} \approx \frac{\sqrt{\tilde{\kappa}_t} - 1}{2} \log \frac{8}{\epsilon_0^2}$$

CG steps, where  $\tilde{\kappa}_t$  is the condition number of  $\tilde{\mathbf{H}}_{t,i}$  and  $\kappa_t$  is the condition number of  $\mathbf{H}_t$ . Then requirement (12) is satisfied and thereby Theorem 4 holds.

**Remark 6** *The best choice of  $\epsilon_0$  is making it comparable to*

$$\vartheta\left(\frac{\epsilon}{m} + \epsilon^2\right),$$

where  $\epsilon = \Theta\left(\frac{\mu d}{s} \log(md)\right)$ . Otherwise, if  $\epsilon_0$  is much larger than  $\vartheta\left(\frac{\epsilon}{m} + \epsilon^2\right)$ , i.e., too few CG steps are taken, the convergence rate is determined by  $\epsilon_0$ . In this case, the advantages of having access to a large local sample size  $s$  are counteracted by such large error in the solution of the local linear system. Conversely, reducing  $\epsilon_0$  much smaller than  $\vartheta\left(\frac{\epsilon}{m} + \epsilon^2\right)$ , i.e., a more exact local solution than what is necessary, will have almost no effect on the convergence, and thus local computations more than necessary are simply wasted. See Section 5.3 for the empirical studies.

It is clear from Corollary 5 that if the condition numbers of the Hessian matrices are large or the local sample size  $s$  is much larger than  $d\mu$ , one should set  $q$  large.

#### 4.4 What Affects the Convergence Rate?

**Effects of  $s$  and  $m$ .** The theory presented in this paper makes explicit the dependence of the convergence on local sample size,  $s$ , and number of partitions (the same to the number of workers),  $m$ . This relationship was not fully captured by the previous works—DANE (Shamir et al. (2014)), AIDE (Reddi et al., 2016), or CoCoA (Jaggi et al., 2014, Ma et al., 2015, Smith et al., 2016). Let us briefly discuss the effects of  $s$ ,  $m$ , and  $n$  is convergence behaviour of GIANT.

- Assume the data are split to disjoint sets; thus the local sample size is  $s = \frac{n}{m}$ . (Line 2 of Algorithm 1 is skipped.) Then  $\frac{\epsilon}{m} \propto \frac{\sqrt{\log m}}{\sqrt{m}}$  and  $\epsilon^2 \propto m \log m$ . Hence, as  $m$  increases,  $\frac{\epsilon}{m} + \epsilon^2$  can increase as well. This implies that larger number of partitions can result in GIANT performing more iterations. The increase in  $m$  may or may not decrease the total elapsed time. It is because as  $m$  grows, the local computational costs decrease (due to smaller  $s$ ), but the number of required iterations can increase.
- Differently, let Line 2 of Algorithm 1 be activated. Assume  $s$  is, irrespective of  $m$ , set to a fixed number, e.g.,  $s = 20d$ . In this case,  $\epsilon$  is also fixed, and, as such, larger  $m$  leads to smaller  $\frac{\epsilon}{m} + \epsilon^2$  and thus faster convergence. In such setting, the increase in  $m$  always leads to less total elapsed time.
- For fixed  $m$ , large values of  $n$  and with  $s = \frac{n}{m}$ , the Hessian matrix is better approximated ( $\epsilon$  is small), and which consequently makes the convergence faster.

Our theories implies that, in practice, if the data are partitioned to disjoint sets, it is crucial to allow for moderately small  $m$  such that  $s = \frac{n}{m}$  is large in comparison with  $d$ . However, this limits the level of parallelism. To make use of a large number of compute nodes, one can activate Line 2 of Algorithm 1 to make the local sample size,  $s$ , large.

**Effects of regularization.** The regularization influences convergence rate in two ways. Firstly, the regularization affects the condition number of the Hessian matrices in each iteration, which in turn influences the convergence. Secondly, large regularization always leads to small  $\vartheta = \frac{\sigma_{\max}^2(\mathbf{A}_t)}{\sigma_{\max}^2(\mathbf{A}_t) + \sigma_{\min}(\mathbf{M})} \leq 1$ . This is indeed intuitive, since for large  $\mathbf{M}$ , the

problem becomes increasingly “quadratic-like”, for which Newton-type methods converge very fast.

**Effects of matrix coherence.** Besides, all previous Newton-type methods considered partitioning the data uniformly at random, which amounts to uniform sampling without replacement for  $m$  times. It is well known that the uniform sampling can be heavily, and negatively, affected by large degrees of heterogeneity in the data. For linear regression, the impact of matrix coherence has been thoroughly studied (Mahoney, 2011, Ma et al., 2014, Wang et al., 2017). Loosely speaking, if the “information” contained in the training data is homogeneously distributed across all samples, i.e., small coherence, then all the solutions to all local problems are equally informative, and hence, such Newton-type methods are expected to perform well. The impact of matrix coherence is readily observed from our empirical study, however, the theoretical analyses in aforementioned prior works have not made such effect explicit.

#### 4.5 Sketch of Proof

Here we outline the main steps of proving the convergence of GIANT; the proofs are left to Appendix C.

Firstly, if the local data are uniformly sampled, either with or without replacement, and the local sample size,  $s$ , is sufficiently large, then the local Hessian matrices  $\tilde{\mathbf{H}}_{t,1}, \dots, \tilde{\mathbf{H}}_{t,m} \in \mathbb{R}^{d \times d}$  well approximate the true Hessian matrix  $\mathbf{H}_t$ . This can be regiously shown using existing “subspace embedding property” of matrix sketching (Drineas et al., 2006b, 2011, Woodruff, 2014). Note that for problem (1), the Hessian matrix  $\mathbf{H}_t$  can be written as  $\mathbf{H}_t = \mathbf{A}_t^T \mathbf{A}_t + \mathbf{M}$  for some  $\mathbf{A}_t \in \mathbb{R}^{n \times d}$ , and the local Hessian matrix  $\tilde{\mathbf{H}}_{t,i}$  can be written as

$$\tilde{\mathbf{H}}_{t,i} = \mathbf{A}_t^T \mathbf{S}_i \mathbf{S}_i^T \mathbf{A}_t + \mathbf{M},$$

where  $\mathbf{S}_i \in \mathbb{R}^{n \times s}$  is a random uniform sampling matrix. For fixed error parameters  $\epsilon, \delta \in (0, 1)$ , if  $s = \Theta(\frac{\mu d}{\epsilon^2} \log \frac{d}{\delta})$ , where  $\mu$  is the row coherence of  $\mathbf{A}_t$ , then

$$(1 - \epsilon) \mathbf{A}_t^T \mathbf{A}_t \preceq \mathbf{A}_t^T \mathbf{S}_i \mathbf{S}_i^T \mathbf{A}_t \preceq (1 + \epsilon) \mathbf{A}_t^T \mathbf{A}_t$$

holds with probability at least  $1 - \delta$ ; see (Woodruff, 2014, Wang et al., 2016). In addition, the average  $\frac{1}{m} \sum_{i=1}^m \mathbf{A}_t^T \mathbf{S}_i \mathbf{S}_i^T \mathbf{A}_t$  is a better approximation to  $\mathbf{A}_t^T \mathbf{A}_t$  (Wang et al., 2017).

Secondly, because  $\tilde{\mathbf{H}}_{t,i}$  well approximates  $\mathbf{H}_t$ , for all  $i \in [m]$ , we can show that the direction

$$\tilde{\mathbf{p}}_t \triangleq \frac{1}{m} \sum_{i=1}^m \tilde{\mathbf{p}}_{t,i} \triangleq \frac{1}{m} \sum_{i=1}^m \tilde{\mathbf{H}}_{t,i}^{-1} \mathbf{g}_t$$

well approximates the true Newton direction  $\mathbf{p}_t^* \triangleq \mathbf{H}_t^{-1} \mathbf{g}_t$ , where  $\mathbf{g}_t$  is the full gradient. This can be quantified by defining the quadratic function

$$\phi_t(\mathbf{p}) \triangleq \frac{1}{2} \mathbf{p}^T \mathbf{H}_t \mathbf{p} - \mathbf{p}^T \mathbf{g}_t,$$

which is non-positive, and showing the bound

$$\phi_t(\mathbf{p}_t^*) \leq \phi_t(\tilde{\mathbf{p}}_t) \leq (1 - \alpha^2) \cdot \phi_t(\mathbf{p}_t^*) \quad \text{holds w.p. at least } 1 - (m + 1)\delta, \quad (13)$$

where  $\alpha = \vartheta \left( \frac{\epsilon}{m} + \frac{\epsilon^2}{1-\epsilon} \right)$  and  $\vartheta = \frac{\sigma_{\max}^2(\mathbf{A}_t)}{\sigma_{\max}^2(\mathbf{A}_t) + \sigma_{\min}(\mathbf{M})} \leq 1$ . Recall that we assume  $s = \Theta\left(\frac{\mu d}{\epsilon^2} \log \frac{d}{\delta}\right)$ ; because here  $\delta$  is in the logarithm, the failure probability in (13) can be small even if  $m$  is very large.

Finally, given (13), we can follow the classical analysis of Newton’s method to show that GIANT enjoys linear-quadratic convergence rate. For non-quadratic loss, we have to assume that the Hessian is  $L$ -Lipschitz, and we can show a local linear-quadratic convergence rate. For quadratic loss, because the Hessian matrix does not changes with the iterations, (equivalently, the Hessian is 0-Lipchitz), we can show a global linear convergence rate.

## 5. Numerical Experiments

In this section we present extensive numerical examples verifying the theories of GIANT. In the process, we will discuss the empirical effects of regularization, problem conditioning, matrix coherence, local sample size, and number of data partition, in the overall performance of GIANT. In Section 5.1, we describe the data and implementations. We evaluate GIANT on two classes of regression problems, linear regression in Section 5.2, followed by logistic regression in Section 5.3.

### 5.1 Settings

**Synthetic data.** Following Ma et al. (2014), Yang et al. (2016), we generate four kinds of data matrices,  $\mathbf{X} \in \mathbb{R}^{n \times d}$ , with different row coherence parameters and condition numbers:

- $\mathbf{X} = \mathbf{U}_C \text{diag}(\boldsymbol{\sigma}_L) \mathbf{V}^T$  is *coherent* and has *low* condition number;
- $\mathbf{X} = \mathbf{U}_C \text{diag}(\boldsymbol{\sigma}_H) \mathbf{V}^T$  is *coherent* and has *high* condition number;
- $\mathbf{X} = \mathbf{U}_I \text{diag}(\boldsymbol{\sigma}_L) \mathbf{V}^T$  is *incoherent* and has *low* condition number;
- $\mathbf{X} = \mathbf{U}_I \text{diag}(\boldsymbol{\sigma}_H) \mathbf{V}^T$  is *incoherent* and has *high* condition number.

Here  $\mathbf{V} \in \mathbb{R}^{d \times d}$  be the orthonormal bases of a  $d \times d$  standard Gaussian matrix; the matrices  $\mathbf{U}_C, \mathbf{U}_I \in \mathbb{R}^{n \times d}$  and vectors  $\boldsymbol{\sigma}_L, \boldsymbol{\sigma}_H \in \mathbb{R}^d$  are described in the following.

We generate the orthonormal bases  $\mathbf{U}_C, \mathbf{U}_I \in \mathbb{R}^{n \times d}$  as follows.  $\mathbf{C} \in \mathbb{R}^{d \times d}$  is the covariance matrix whose the  $(i, j)$ -th entry is  $2 \times 0.5^{|i-j|}$ .  $\mathbf{B}_I \in \mathbb{R}^{n \times d}$  is the incoherent matrix whose rows are sampled from multivariate normal  $\mathcal{N}(\mathbf{1}_d, \mathbf{C})$ , and  $\mathbf{U}_I \in \mathbb{R}^{n \times d}$  is the orthonormal bases of  $\mathbf{B}_I$ .  $\mathbf{B}_C \in \mathbb{R}^{n \times d}$  is the coherent matrix whose rows are sampled from multivariate Student’s t-distribution with covariance matrix  $\mathbf{C}$  and  $\nu = 4$  degree of freedom, and, finally,  $\mathbf{U}_C \in \mathbb{R}^{n \times d}$  is the orthonormal bases of  $\mathbf{B}_C$ .

We generate the singular values of  $\mathbf{X}$  as follows. Let  $\mathbf{a} \in \mathbb{R}^d$  be the vector of  $d$  linearly equally spaced points between 0 and  $-1$ , and let  $\boldsymbol{\sigma}_L \in \mathbb{R}^d$  be the vector whose the  $i$ -th entry is  $10^{a_i}$ . We generate  $\boldsymbol{\sigma}_H \in \mathbb{R}^d$  in the same way except that  $\mathbf{a}$  is linearly equally spaced points between 0 and  $-8$ .

**Real-world data.** For linear regression, we use the Year Prediction Million Song Data (MSD), which has  $n = 463,715$  training samples and  $d = 90$  features. For logistic regression, we use three binary classification datasets: covtype ( $n = 581,012$  and  $d = 54$ ), w8a ( $n = 49,749$  and  $d = 300$ ), and a9a ( $n = 32,561$  and  $d = 123$ ). The data can be

downloaded from <http://www.csie.ntu.edu.tw/~cjlin/libsvmtools/datasets/>. The features of the data are scaled to  $[-1, 1]$ .

**Kernel regression and classification.** In addition, because for the four datasets, the number of features,  $d$ , is too small, we apply GIANT to kernel regression and classification tasks where we use higher dimensional features. In practice, high dimensional features help improve training and testing errors; but here our only focus is the optimization objective, and we do not study training and testing errors. We generate  $r = 1,000$  random Fourier feature (Rahimi and Recht, 2007) of the RBF kernel  $\kappa(\mathbf{x}_i, \mathbf{x}_j) = \exp\left(-\frac{1}{2\sigma^2}\|\mathbf{x}_i - \mathbf{x}_j\|_2^2\right)$ . We set

$$\sigma = \sqrt{\frac{1}{n^2} \sum_{i=1}^n \sum_{j=1}^n \|\mathbf{x}_i - \mathbf{x}_j\|_2^2}.$$

The random features are generated in the following way. Let  $\mathbf{R} \in \mathbb{R}^{d \times r}$  be a matrix with each entry randomly and independently drawn from  $\mathcal{N}(0, 1/\sigma^2)$  and  $\mathbf{q} \in \mathbb{R}^r$  be a vector with each entry randomly and independently drawn from the uniform distribution  $[0, 2\pi]$ . Let  $\mathbf{X} \in \mathbb{R}^{n \times d}$  be the raw input and  $\mathbf{Z} = \sqrt{2} \cos(\mathbf{X}\mathbf{R} + \mathbf{1}_n \mathbf{q}^T) \in \mathbb{R}^{n \times r}$  be the random features, where  $\cos(\cdot)$  is applied elementwisely to the matrix. We use  $\mathbf{Z}$  in lieu of the smaller matrix  $\mathbf{X}$  in the regression problem.

**Implementation.** We implement GIANT and the compared methods using Python and run the code in MacBook Pro 2015 for numerical simulations. The Python code is available at <https://github.com/wangshusen/GIANT-Python-Code.git>. To solve large-scale dense problems, the users can use our Apache Spark implementation available at <https://github.com/wangshusen/SparkGiant.git>.

**Line search.** Wherever line search is applied, we use Armijo rule, select the step size from  $\{4^0, 4^{-1}, \dots, 4^{-9}\}$ , and fix the control parameter to  $c = 0.1$ . These line search parameters are problem-independent and data-independent and do not need tuning. According to our off-line experiments, the tuning of these parameter does not demonstrate substantial improvement to the convergence.

## 5.2 Experiments on Linear Regression

We conduct medium-scale experiments on the least squares regression and ridge regression to verify the theories presented in this paper. Section 5.2.1 presents empirical results on the synthetic data followed by discussions on the theory and observed empirical results in Section 5.2.2. Experiments with real data are given in Section 5.2.3. Note that for quadratic loss, we do not compare with DANE (Shamir et al., 2014) or AIDE (Reddi et al., 2016), as in this case, they are basically equivalent to GIANT, but our evaluation here is much more detailed than what has been presented previously.

### 5.2.1 EXPERIMENTS ON SYNTHETIC DATA

**Data for linear regression.** Let  $\mathbf{X}$  be defined in Section 5.1. Let  $\mathbf{w} = [\mathbf{1}_{0.2d}; 0.1 \mathbf{1}_{0.6d}; \mathbf{1}_{0.2d}]$  and  $\mathbf{y} = \mathbf{X}\mathbf{w} + \boldsymbol{\xi}$ , where each entry of  $\boldsymbol{\xi}$  is independently sampled from  $\mathcal{N}(0, 0.1^2)$ .

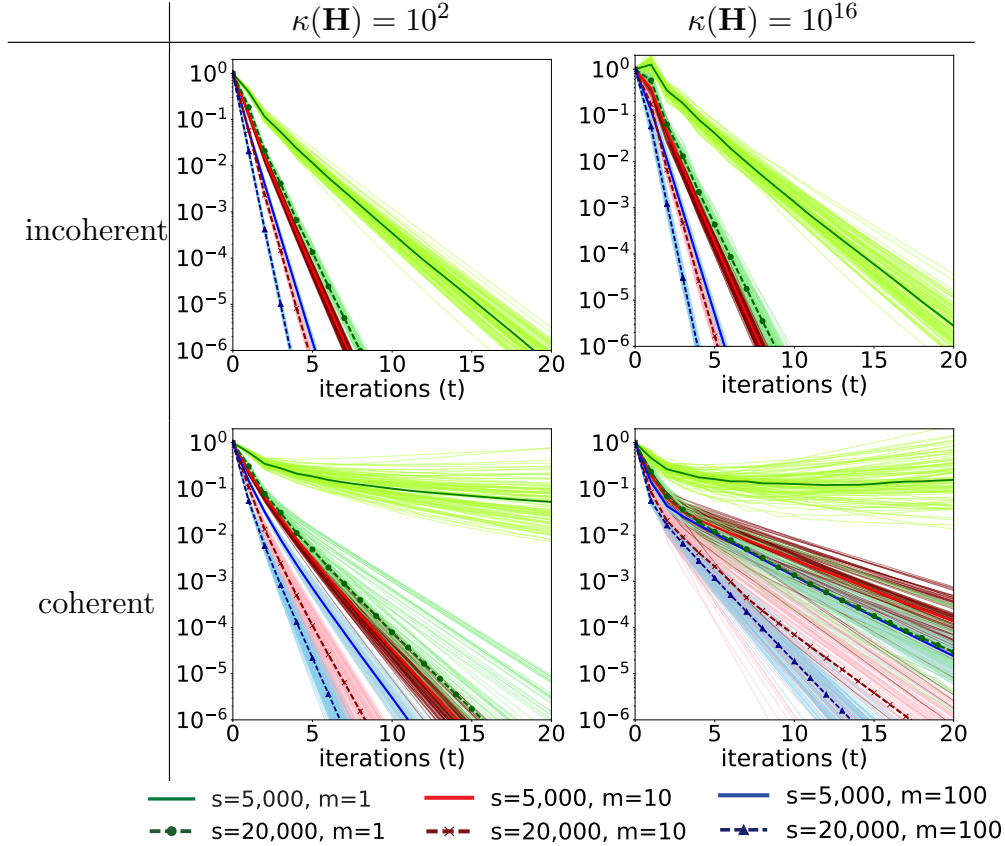


Figure 2: Least squares regression on synthetic data sets with  $n = 2 \times 10^5$  and  $d = 200$ . The  $x$ -axis is number of iterations; the  $y$ -axis is the ratio  $\frac{\|\mathbf{w}_t - \mathbf{w}^*\|_2}{\|\mathbf{w}^*\|_2}$ . Each of the  $m$  worker machines uses  $s$  samples to approximate the Hessian matrix. A thin curve represents one trial; a thick curve represents the medians of each of the 100 trials under one setting of  $(s, m)$ .

**Settings.** We set  $n = 200,000$  and  $d = 200$ , and initialize with  $\mathbf{w}_0 = \mathbf{0}$ . Let  $\mathbf{w}^*$  be the optimal solution found by the SVD of  $\mathbf{X}$ ;  $\mathbf{w}_t$  be the output of the  $t$ -th iteration. Given the local data and full gradient, the local Newton directions are computed exactly by the inversion of the Hessian matrix. Because the data partition is random, for each setting of  $s$  and  $m$ , we repeat experiments 100 times and plot all the  $\|\mathbf{w}_t - \mathbf{w}^*\|_2$  and their median.

**Least squares regression.** We use GIANT to solve the least squares regression problem  $\operatorname{argmin}_{\mathbf{w}} \|\mathbf{X}\mathbf{w} - \mathbf{y}\|_2^2$ . The local sample size  $s$  are chosen as 5,000 or 20,000 and number of nodes  $m$  is set to 1, 10, or 100. We plot the distance  $\|\mathbf{w}_t - \mathbf{w}^*\|_2$  as thin lines in Figure 2; we also plot the medians as thick lines or dashes.

**Ridge regression.** We then apply GIANT to solve the ridge regression problem

$$\operatorname{argmin}_{\mathbf{w}} \frac{1}{2n} \|\mathbf{X}\mathbf{w} - \mathbf{y}\|_2^2 + \frac{\gamma}{2} \|\mathbf{w}\|_2^2, \quad (14)$$

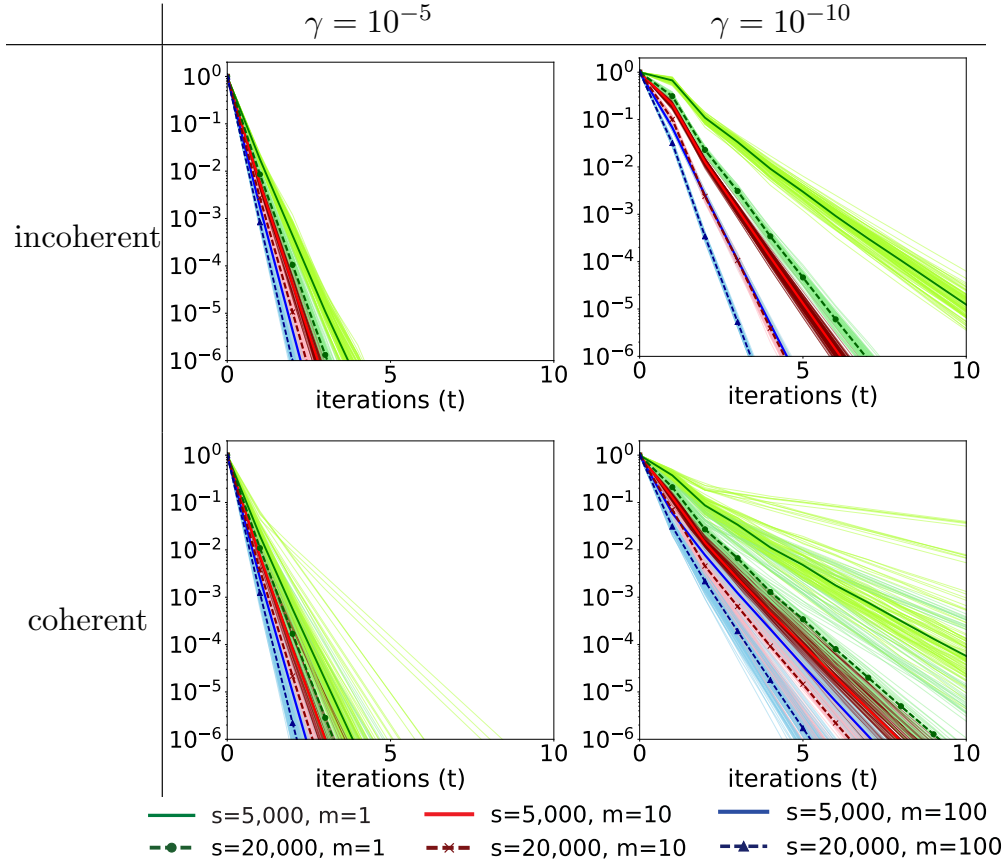


Figure 3: Ridge regression on the ill-conditioned synthetic data sets with  $n = 2 \times 10^5$  and  $d = 200$ . The  $x$ -axis is number of iterations; the  $y$ -axis is the ratio  $\frac{\|\mathbf{w}_t - \mathbf{w}^*\|_2}{\|\mathbf{w}^*\|_2}$ . Each of the  $m$  worker machines uses  $s$  samples to approximate the Hessian matrix. A thin curve represents one trial; a thick curve represents the medians of each of the 100 trials under one setting of  $(s, m)$ .

where  $\gamma$  is the regularization parameter. The Hessian matrix is  $\mathbf{H} = \mathbf{X}^T \mathbf{X} + n\gamma \mathbf{I}_d$ ; large  $\gamma$  leads to small condition number  $\kappa(\mathbf{H})$ . We use the data with high condition number ( $\kappa(\mathbf{X}^T \mathbf{X}) = 10^{16}$ ). We conduct three sets of experiments.

- First, as before, we set the local sample sizes  $s$  to be 5,000 or 20,000, number of partitions  $m$  to be 1, 10, or 100, and report the results in Figure 3. Here Newton’s step size is set to one and no line-search is used.
- Second, we set  $s$  as a function of  $m$  by letting  $s = \frac{n}{m}$  (data partition without overlap) and report the results in Figure 4. Here Newton’s step size is set to one and no line-search is used.
- Third, we set  $m = 16, 128, \text{ or } 1024$ ,  $s = \frac{n}{m}$ , and compare fixed step size with line search and plot the results in Figure 5.

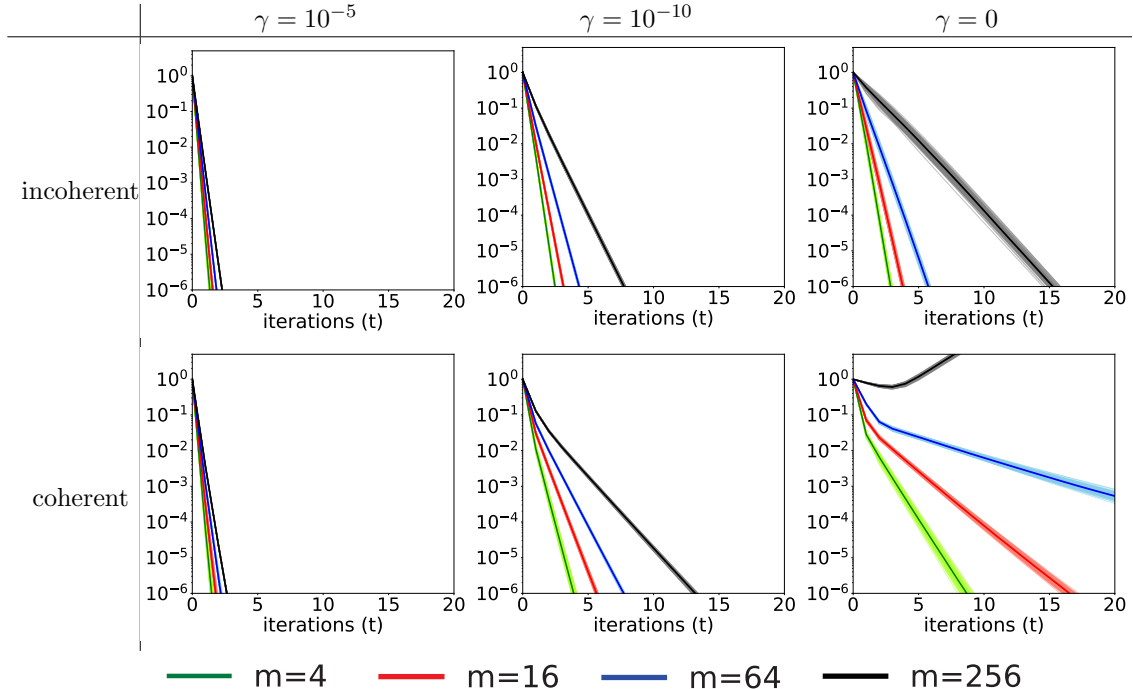


Figure 4: Ridge regression on the ill-conditioned synthetic data sets with  $n = 2 \times 10^5$  and  $d = 200$ . The  $x$ -axis is number of iterations; the  $y$ -axis is the ratio  $\frac{\|\mathbf{w}_t - \mathbf{w}^*\|_2}{\|\mathbf{w}^*\|_2}$ . The  $n$  samples are split among  $m$  machines, and each machine holds  $s = \frac{n}{m}$  samples. A thin curve represents one trial; a thick curve represents the medians of each of the 100 trials under one setting of  $m$ .

### 5.2.2 DISCUSSIONS

In light of the experiments of Section 5.2.1, we now discuss the effects of the condition number, regularization, coherence, local sample size  $s$ , number of partitions  $m$ , and line search.

**Effect of condition number.** Figure 2 shows that the condition number  $\kappa(\mathbf{H})$  has small impact on the convergence of GIANT as suggested by Theorem 1 (this is indeed expected for quadratic models, e.g., Roosta-Khorasani and Mahoney (2016a,b), Xu et al. (2016)). This is in sharp contrast to the theory of DANE (Shamir et al., 2014) and AIDE (Reddi et al., 2016), for which, to reach a fixed error  $\|\mathbf{w}_t - \mathbf{w}^*\|_2 \leq \mathcal{E}$ , the number of iterations  $t$  is predicted to be proportional to  $\kappa^2(\mathbf{H})$  or  $\sqrt{\kappa(\mathbf{H})}$ , which does not match our empirical results. (Note that DANE and AIDE are basically equivalent to GIANT in the linear regression case.) Our results indicates that DANE’s and AIDE’s dependence of the condition number is likely artifact of their analysis.

**Effect of regularization,  $\gamma$ .** In Figures 3, 4, and 5, we observe that larger  $\ell_2$  regularizer  $\gamma\|\mathbf{w}\|_2^2$  always leads to faster convergence. This observation agrees with Theorem 1: larger

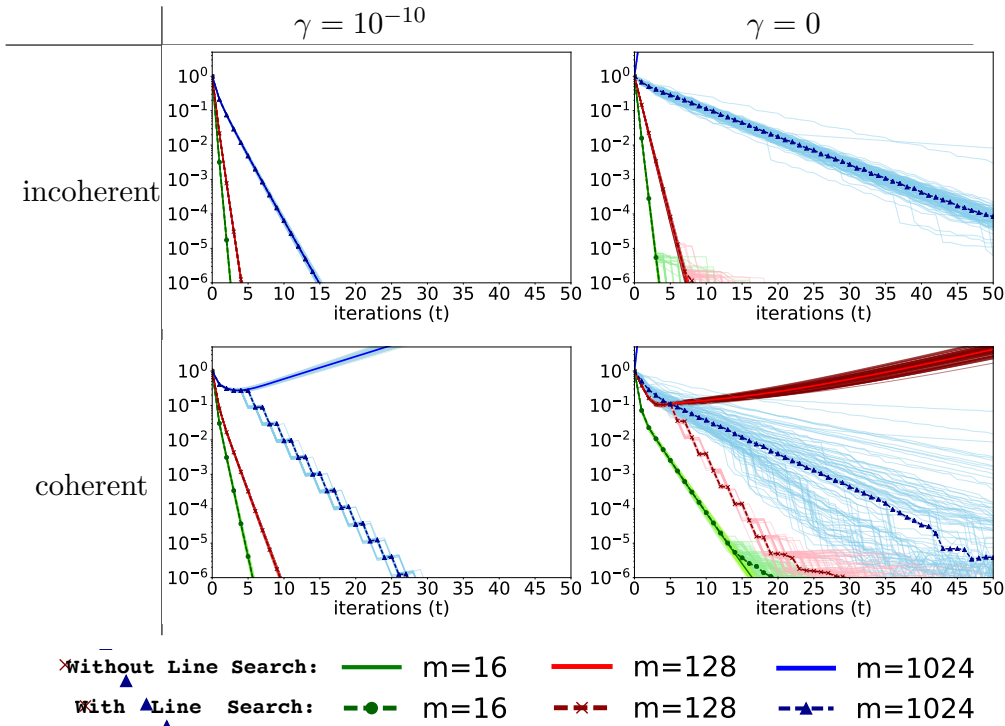


Figure 5: Ridge regression on the ill-conditioned synthetic data sets with  $n = 2 \times 10^5$  and  $d = 200$ . The  $x$ -axis is number of iterations; the  $y$ -axis is the ratio  $\frac{\|w_t - w^*\|_2}{\|w^*\|_2}$ . The  $n$  samples are split among  $m$  machines, and each machine holds  $s = \frac{n}{m}$  samples. A thin curve represents one trial; a thick curve represents the medians of each of the 100 trials under one setting of  $m$ .

$\gamma$  implies smaller  $\vartheta = \frac{\sigma_{\max}^2(\mathbf{X})}{\sigma_{\max}^2(\mathbf{X}) + n\gamma}$ , which in turn predicts faster convergence. In addition, as  $\gamma$  gets bigger, the condition number of  $\mathbf{H} = \frac{1}{n}\mathbf{X}^T\mathbf{X} + \gamma\mathbf{I}_d$  becomes smaller, which can make convergence a little faster.

**Effect of matrix coherence,  $\mu$ .** In Figures 2, 3, 4, and 5, we always observe that for fixed condition number  $\kappa$ , regularization  $\gamma$ , number of partition  $m$ , and local sample size  $s$ , GIANT converges faster on the incoherent data than the coherent. This verifies our theory: for fixed  $s$ , large  $\mu$  leads to coarse approximation of the Hessian matrix and thus slower convergence. The effect of matrix coherence has not been explicitly captured by the analysis in the previous similar works (Reddi et al., 2016, Shamir et al., 2014, Smith et al., 2016, Zhang and Lin, 2015).

**Effect of number of partitions,  $m$ .** Theorem 1 shows that the convergence is fast if  $\frac{\epsilon}{m} + \epsilon^2$  is small, where  $\epsilon^2 = \Theta(\frac{\mu d}{s} \log(md))$ . Therefore, large  $m$  generally leads to small  $\frac{\epsilon}{m} + \epsilon^2$  and thus fast convergence. From Figures 2 and 3, it is clear that for a fixed local sample size,  $s$ , large values of  $m$  always leads to fast convergence, which matches our theory.

However, if we set  $s = \frac{n}{m}$  rather than fixing  $s$ , then  $\epsilon^2 = \Theta(\frac{\mu dm}{n} \log(md))$ . Thus as  $m$  grows,  $\frac{\epsilon}{m} + \epsilon^2$  can grow as well, making the convergence slower (in terms of the number of iterations, not the total elapsed time). From Figures 4 and 5, we see that under the setting of  $s = \frac{n}{m}$ , large  $m$  always yields slow convergence in terms of iterations.

**Effect of local sample size,  $s$ .** Figures 2 and 3 show that for a fixed  $m$  (number of partitions), large  $s$  clearly leads to fast convergence, as predicted by the theory developed in this paper.

**Effect of line search.** As our theory predicts, when the local sample size is sufficiently large compared to  $d$ , GIANT with fixed step size  $\beta_t = 1$  is guaranteed to converge. In Figure 5, GIANT with big  $s = \frac{n}{m}$  and fixed step size always converges. In contrast, when  $m = 1024$ , the local sample size  $s = \frac{n}{m} = 195$  is smaller than  $d = 200$ ; consequently, the blue lines (without marker) in Figure 5 mostly diverge. In contrast, under the same setting where  $s < d$ , the use of line search in GIANT always leads to convergence; in particular, with slight regularization  $\gamma = 10^{-10}$ , GIANT with line search converges very rapidly.

### 5.2.3 EXPERIMENTS ON REAL-WORLD DATA

We conduct experiments on the Year Prediction Million Song Data (MSD), which has  $n = 463,715$  training samples and  $d = 90$  features. In addition, because  $d = 90$  is too small compared to  $n = 463,715$ , we generate  $r = 1000$  random Fourier feature (Rahimi and Recht, 2007).

We use the 90-dimensional raw input and the 1000-dimensional random Fourier features, respectively, for the ridge regression problem (14). We vary the regularization parameter  $\gamma$  and the number of partitions  $m$  but fix  $s = \frac{n}{m}$ . We use backtracking line search. For the raw input, we repeat experiments 100 times; for the random features, because the experiments are much more expensive, we only repeat 20 times. The results are reported in Figure 6.

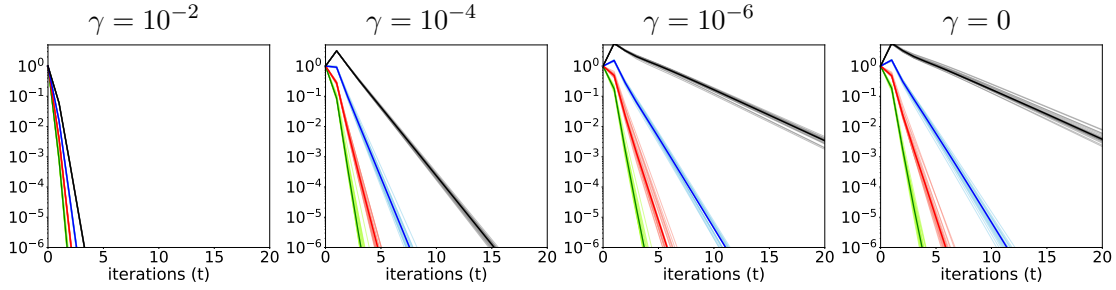
The results with the real-world data are analogous to those with the synthetic data. With a reasonable regularization, e.g.,  $\gamma = 10^{-4}$ , GIANT with line search converges to a very high precision in a small number of iterations. Using  $m = 256$  partitions, each worker only holds  $s = 1811$  samples, which is only slightly bigger than 1000 (number of random Fourier features). Even under such setting, GIANT demonstrates satisfactory convergence behavior.

## 5.3 Experiments on Logistic Regression

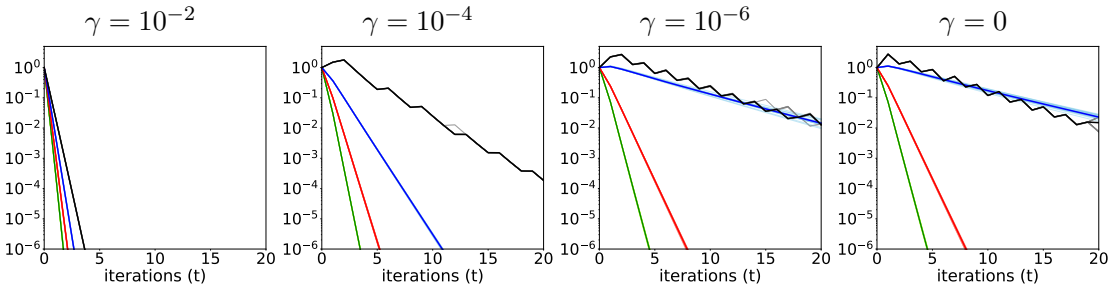
To qualitatively verify the theory presented in this paper, we now present medium-scale experiments on the logistic regression with  $\ell_2$  regularization, i.e.,

$$\operatorname{argmin}_{\mathbf{w}} \frac{1}{n} \sum_{j=1}^n \log(1 + \exp(-y_j \mathbf{x}_j^T \mathbf{w})) + \frac{\gamma}{2} \|\mathbf{w}\|_2^2, \quad (15)$$

where  $\mathbf{x}_j \in \mathbb{R}^d$  is a feature vector and  $y_j \in \{-1, +1\}$  is the corresponding response.



(a) Experiments on the 90-dimensional raw input.



(b) Experiments on the 1000-dimensional random Fourier features.

—  $m=4$     —  $m=16$     —  $m=64$     —  $m=256$

Figure 6: Ridge regression on the Million Song Data and its random Fourier features. The  $x$ -axis is number of iterations; the  $y$ -axis is the ratio  $\frac{\|\mathbf{w}_t - \mathbf{w}^*\|_2}{\|\mathbf{w}^*\|_2}$ . The  $n = 463,715$  samples are split among  $m$  machines, and each machine holds  $s = \frac{n}{m}$  samples. A thin curve represents one trial; a thick curve represents the medians of each of all the trials under one setting of  $m$ .

### 5.3.1 EXPERIMENTS ON SYNTHETIC DATA

We generate a set of synthetic data in the following way. The feature matrix  $\mathbf{X} \in \mathbb{R}^{n \times d}$  is the same coherent and ill-conditioned matrix as in Section 5.1. Let  $\mathbf{w} = [\mathbf{1}_{0.2d}; 0.1 \mathbf{1}_{0.6d}; \mathbf{1}_{0.2d}]$ . For  $j \in [n]$ , let  $p_j = \frac{\exp(\mathbf{w}^T \mathbf{x}_j)}{1 + \exp(\mathbf{w}^T \mathbf{x}_j)}$  and sample  $y_j$  according to the binomial distribution  $\mathbb{P}\{Y_j = +1\} = p_j$  and  $\mathbb{P}\{Y_j = -1\} = 1 - p_j$ . In this way, we get a balanced dataset which has about 50% positive samples and 50% negative samples. We set  $n = 200,000$  and  $d = 1,000$ .

The same as before, we initialize with  $\mathbf{w}_0 = \mathbf{0}$ . In each iteration, each worker finds its local Newton direction by taking  $q$  CG steps. We use different settings of  $q$  and the regularization parameter  $\gamma$ . We randomly partition the  $n$  data samples to  $m$  disjoint sets and repeat this procedure 10 times. The convergence curves of the 10 repeats are reported as thin lines and their medians as thick lines. In this way, the local sample sizes are given as  $s = \frac{n}{m}$ . Backtracking line search is applied to determine step size.

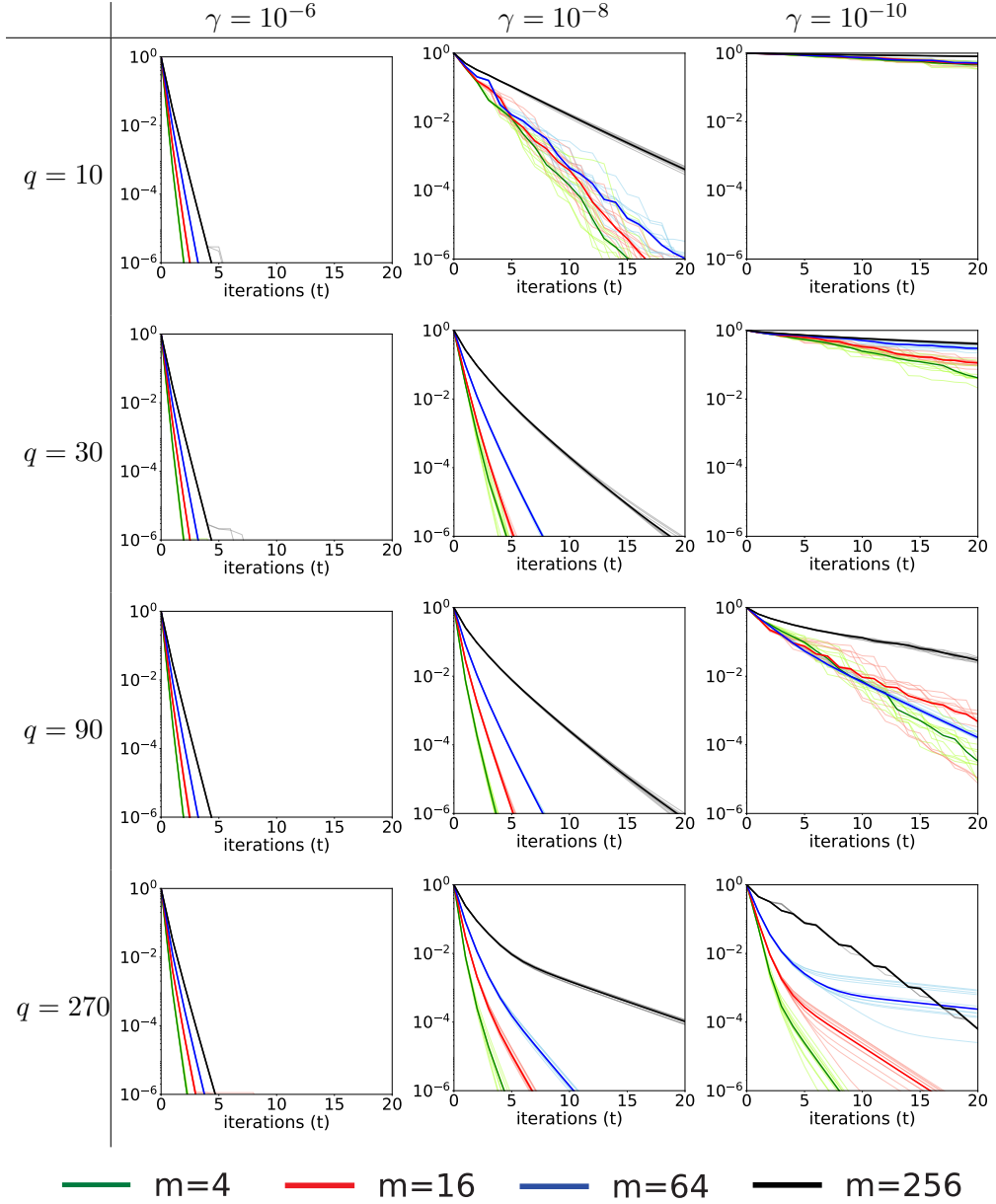


Figure 7: Logistic regression on synthetic data sets with  $n = 2 \times 10^5$  and  $d = 10^3$ . The  $x$ -axis is number of iterations; the  $y$ -axis is the ratio  $\frac{\|\mathbf{w}_t - \mathbf{w}^*\|_2}{\|\mathbf{w}^*\|_2}$ . The  $n$  samples are split among  $m$  machines, and each machine holds  $s = \frac{n}{m}$  samples;  $q$  denotes the number of CG steps. For the three choices of  $\gamma$ , the condition numbers of  $\mathbf{H}^*$  are respectively 2.3, 125.7, and 12451.

Here, we aim to empirically study the effects of the following factors: (a) number of partitions  $m$ , (b) the number of local CG iterations  $q$ , and (c) regularization parameter  $\gamma$ .

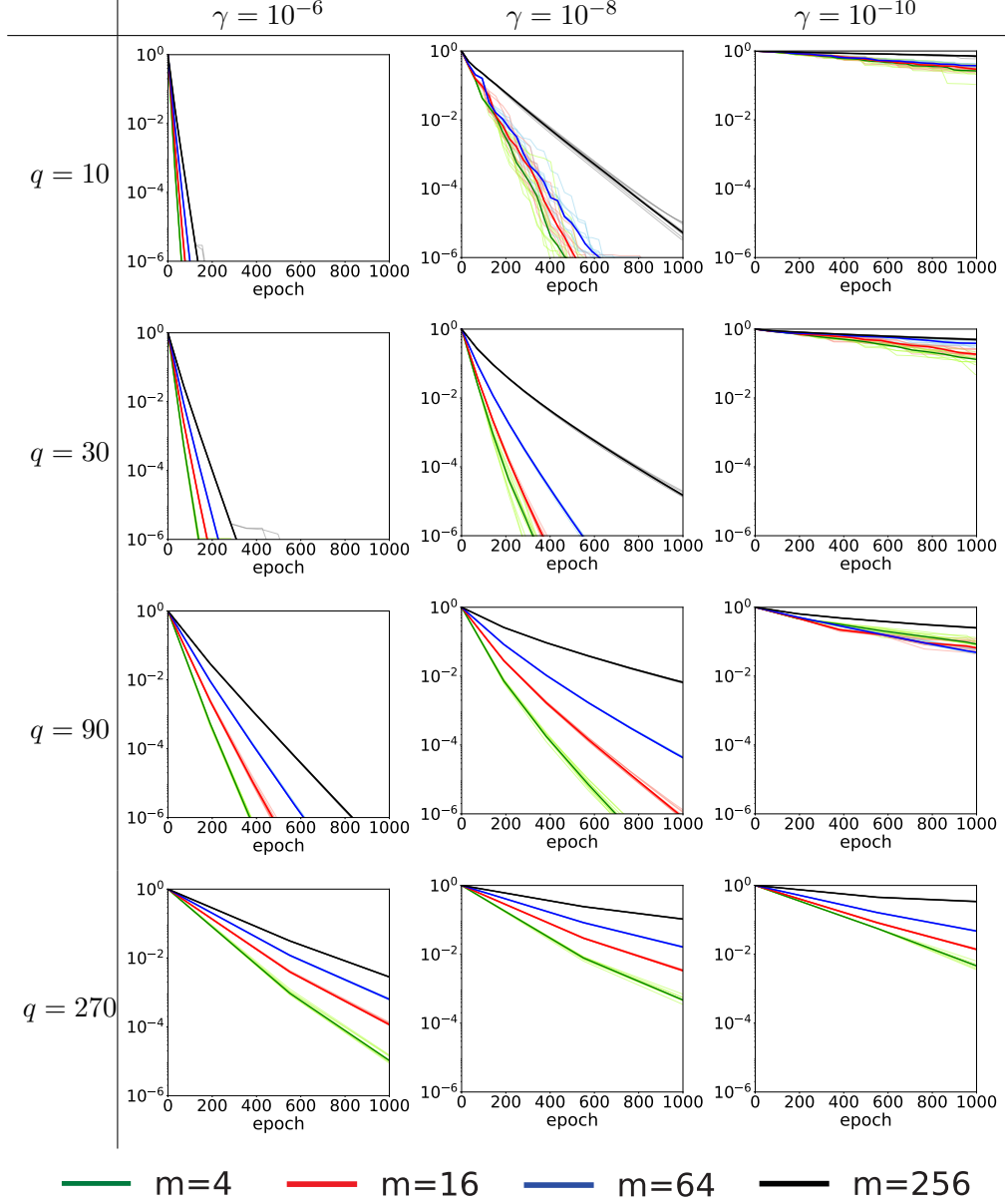


Figure 8: Logistic regression on synthetic data sets with  $n = 2 \times 10^5$  and  $d = 10^3$ . The  $x$ -axis is number of epochs (number of passes through the local data); the  $y$ -axis is the ratio  $\frac{\|\mathbf{w}_t - \mathbf{w}^*\|_2}{\|\mathbf{w}^*\|_2}$ . The samples are split among  $m$  machines, and each machine holds  $s = \frac{n}{m}$  samples;  $q$  denotes the number of CG steps. For the three choices of  $\gamma$ , the condition numbers of  $\mathbf{H}^*$  are respectively 2.3, 125.7, and 12451

Recall from Theorem 4 that

$$\|\Delta_{t+1}\|_2 \leq \max \left\{ \left( \vartheta \frac{\epsilon}{m} + \vartheta \epsilon^2 + \epsilon_0 \right) \sqrt{\frac{\sigma_{\max}(\mathbf{H}_t)}{\sigma_{\min}(\mathbf{H}_t)}} \|\Delta_t\|_2, \frac{L}{\sigma_{\min}(\mathbf{H}_t)} \|\Delta_t\|_2^2 \right\}. \quad (16)$$

Here  $\Delta_t = \mathbf{w}_t - \mathbf{w}^*$  is the error in the solution at  $t$ -th iteration. Since, for a given data set  $(\mathbf{X}, \mathbf{y})$ , the quantities  $L, n, d$  are fixed, in principle, one should observe the following convergence behaviors:

1. Recall that  $\epsilon^2 = \tilde{\Theta}\left(\frac{d\mu_t}{s}\right) = \tilde{\Theta}\left(\frac{md\mu_t}{n}\right)$  where  $\mu_t > 1$  is some parameter depending on the data and  $\mathbf{w}_t$ . Therefore

$$\frac{\epsilon}{m} + \epsilon^2 \geq 2\sqrt{\frac{\epsilon^3}{m}} = \tilde{\Theta}(m^{1/4}),$$

which implies that, as the number of partition  $m$  grows, the error  $\frac{\epsilon}{m} + \epsilon^2$  usually becomes larger, and, in turn, the convergence gets *slower* in terms of iterations.

2. Note that the error parameter  $\epsilon_0$  is proportional to  $\left(\frac{\sqrt{\kappa_t}-1}{\sqrt{\kappa_t}+1}\right)^q$ , where  $\kappa_t = \frac{\sigma_{\max}(\mathbf{H}_t)}{\sigma_{\min}(\mathbf{H}_t)}$  is the condition number of  $\mathbf{H}_t$  and  $q$  is the number of local CG steps. As  $q$  increases, the error  $\epsilon_0$  decreases exponentially, and fewer number of iterations  $t$  is required for convergence.
3. As the regularization parameter  $\gamma$  grows, the parameters  $\vartheta, \sqrt{\kappa_t}, \frac{L}{\sigma_{\min}(\mathbf{H}_t)}$ , and  $\epsilon_0 \propto \left(\frac{\sqrt{\kappa_t}-1}{\sqrt{\kappa_t}+1}\right)^q$  all decrease, and thus the convergence gets *faster*.

We vary  $m, \gamma$ , and  $q$  to study their impact on convergence. In Figure 7 we plot the error  $\|\Delta_t\|_2 = \|\mathbf{w}_t - \mathbf{w}^*\|_2$  against the number of iterations  $t$ . All the empirical results corroborate the above theoretical predictions on the effect of  $m, \gamma$ , and  $q$ .

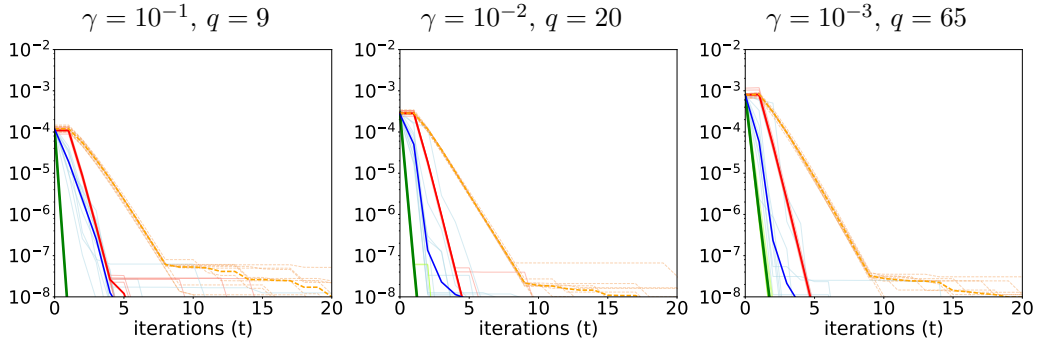
In Figure 8 we plot the error  $\|\Delta_t\|_2$  against the local computations quantified by ‘‘epochs’’. One epoch constitutes one full pass, by each worker, through its local data; in other words, one epoch means that every sample has been seen exactly once by the algorithm. Computing the full gradient  $\mathbf{g}_t$  requires 2 epochs; solving the local Newton direction takes  $q$  CG steps and thus  $2q$  epochs; the line search evaluates the objective value at 10 different points and thus requires 10 epochs. In total, in each iteration,  $12 + 2q$  epochs are required. As for the amount of local computations, for  $\gamma$  set as  $10^{-6}, 10^{-8}$ , and  $10^{-10}$ , the most appropriate choices for the maximum number of CG iterations  $q$  were found to be 10, 30 and 270, respectively. Indeed,  $q$  should be chosen according to the condition number of the Hessian matrices.

Figures 7 and 8 together show that  $q$  implies a trade-off between communication and local computation. A large  $q$  leads to fast convergence in terms of iteration and communication (each iteration has 6 rounds communication). However, a large  $q$  also implies more local computations, which may lead to slow convergence in terms of computation.

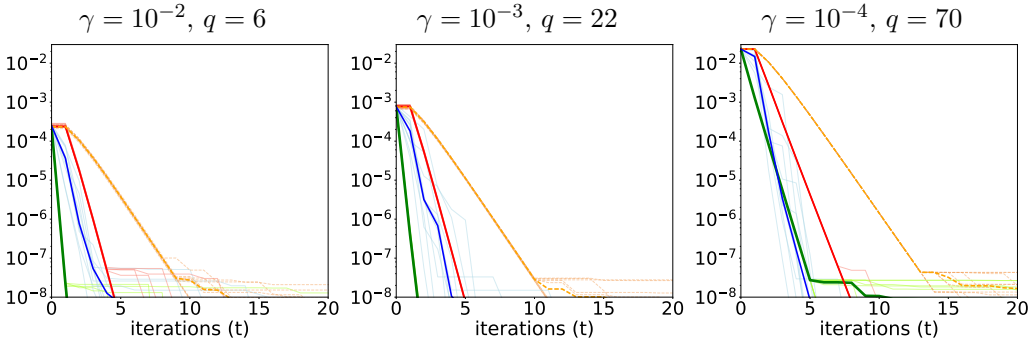
### 5.3.2 COMPARING WITH DANE AND AIDE

**Compared methods.** We empirically compare GIANT with the inexact variants of DANE (Reddi et al., 2016, Shamir et al., 2014) and AIDE (Reddi et al., 2016). We report the results in Figures 9, 10, and 11. In the following, we will simply refer to the inexact DANE as DANE. We do not compare with CoCoA<sup>+</sup> (Ma et al., 2015) and DiSCO (Zhang and Lin, 2015) for the following reasons.

- If the partition is by data, CoCoA<sup>+</sup> solves the dual problem, and it is thus not so straightforward to plot the convergence of the primal error  $\|\mathbf{w}_t - \mathbf{w}^*\|_2$ , across all



(a) Experiments on the 54-dimensional raw input. For the three settings of  $\gamma$ , the condition numbers of  $\mathbf{H}^*$  are respectively 8.8, 74.5, and 646.4.



(b) Experiments on the 1000-dimensional random Fourier features. For the three settings of  $\gamma$ , the condition numbers of  $\mathbf{H}^*$  are respectively 10.5, 87.2, and 749.7.

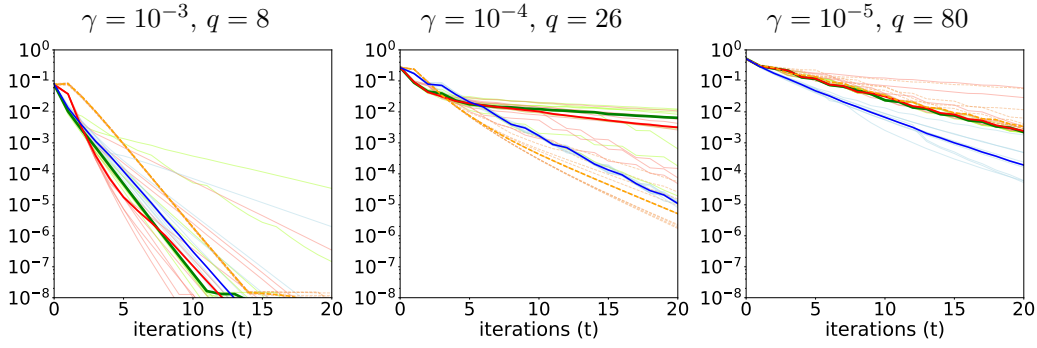
— GIANT    — DANE    — AIDE ( $\tau = 0.1$ )    - - - AIDE ( $\tau = 1$ )

Figure 9: Logistic regression on the Covtype data and its random Fourier features. The  $x$ -axis is number of iterations; the  $y$ -axis is the ratio  $\frac{\|\mathbf{w}_t - \mathbf{w}^*\|_2}{\|\mathbf{w}^*\|_2}$ . The  $n = 581,012$  are randomly split to  $m = 16$  machines, and each machine holds  $s = \frac{n}{m} = 36,313$  samples.  $\tau$  is the parameter of AIDE.

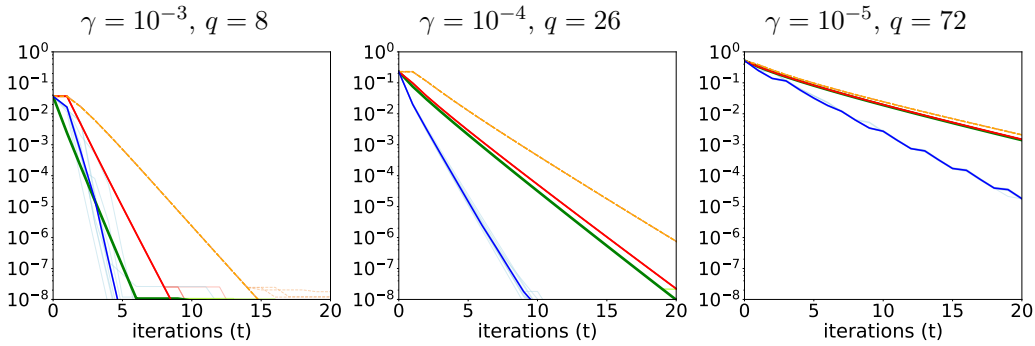
iterations. Importantly, experiments in (Reddi et al., 2016) have shown that DANE and AIDE significantly outperform CoCoA<sup>+</sup> for logistic regression tasks. Besides, CoCoA<sup>+</sup> requires locally solving the dual of logistic regression, which is a constrained problem and cannot be solved as efficiently as an unconstrained problem.<sup>8</sup>

- Each iteration of the inner loop of DiSCO requires the exact solution to a  $d \times d$  linear system for the sake of preconditioning. It unknown whether DiSCO with the linear system approximately solved is guaranteed to converge. Consequently, to make a fair comparison, GIANT, DANE, and AIDE must solve their local problems exactly, which is inefficient. In addition, DiSCO solves the  $d \times d$  linear system by the driver machine,

8. The CoCoA papers solved SVM. Using coordinate descent, their subproblems has closed-form update formular. This is not the case for logistic regression.



(a) Experiments on the 300-dimensional raw input. For the three settings of  $\gamma$ , the condition numbers of  $\mathbf{H}^*$  are respectively 15.7, 112.9, and 969.6.



(b) Experiments on the 1000-dimensional random Fourier features. For the three settings of  $\gamma$ , the condition numbers of  $\mathbf{H}^*$  are respectively 15.1, 118.4, and 796.0.

— GIANT    — DANE    — AIDE ( $\tau = 0.1$ )    - - - AIDE ( $\tau = 1$ )

Figure 10: Logistic regression on the w8a data and its random Fourier features. The  $x$ -axis is number of iterations; the  $y$ -axis is the ratio  $\frac{\|\mathbf{w}_t - \mathbf{w}^*\|_2}{\|\mathbf{w}^*\|_2}$ . The  $n = 49,749$  are randomly split to  $m = 16$  machines, and each machine holds  $s = \frac{n}{m} = 3109$  samples.  $\tau$  is the parameter of AIDE.

and meanwhile the workers are idle. Unless  $d$  is very small, the parallelism of DiSCO is poor. In sum, it is difficult to fairly compare DiSCO with GIANT, DANE, and AIDE, in terms of either local computation and global communication.

**Settings.** DANE and AIDE are briefly reviewed in Appendix B. The compared methods are set in the following way.

- **Local solvers.** Each worker of DANE solves a logistic regression problem using the local data. We use mini-batch SVRG with batch size 100, which is a variant of (Johnson and Zhang, 2013), to solve the local problem. We set the iterations of the inner loop of SVRG to  $s$ ; in this way, each iteration of SVRG amounts to 2 epochs, which is the same to the per-iteration cost of CG. We choose learning rate from  $\{0.1, 1, 10\}$  and report the best.

- **Epochs.** Recall that one epoch means that every data has been seen exactly once. For all the three methods, we vary the number of iterations of the local sub-problems (denote  $q$ ). Note that for the three methods, one iteration amounts to  $2q + 12$  epochs.<sup>9</sup> Also note that each iteration costs 6 rounds of communications. For the three methods, each iteration has the same number of communications and epochs, and thus using the number of iterations as the  $x$ -axis in the convergence plots is fair. The number of local iterations is set by the rule  $q = \frac{\sqrt{\kappa}-1}{2} \log \frac{8}{\epsilon_0}$ . Here  $\kappa$  is the condition number of the Hessian matrices at  $\mathbf{w}^*$ ,<sup>10</sup> and  $\epsilon_0$  is set to 0.2 (somehow arbitrarily).
- **Line search.** In our off-line experiments, when the local sample size  $s$  is not sufficiently larger than  $d$ , we observe that line search is necessary to guarantee convergence of the three compared methods. Therefore, after computing a descending direction, we use line search to determine the step size.
- **Parameters of DANE and AIDE.** Besides the choice of algorithm, DANE has 2 additional parameters  $\eta_1$  and  $\eta_2$ . We select  $\eta_1$  from  $\{0.5, 1\}$  and use the better. We set  $\eta_2 = 0$  because we use line search. Note that DANE is a subroutine of AIDE. For AIDE, the parameters of DANE are set in the same way. AIDE has an additional parameter  $\tau$  (see Appendix B), which we choose from  $\{0.1, 1\}$  and report both results.
- **Initialization.** The three methods are all initialized by model averaging (Zhang et al., 2013), that is, each worker solves a local problem, and the driver uses the averaged solution as the initialization. The local problems are all solved by mini-batch SVRG using  $2q$  epochs. Note that model averaging is not necessary; in our off-line experiments, all the compared methods with zero initialization work very well. In contrast, model averaging can save one or two iterations.

Clearly, GIANT is much easier to tune than DANE and AIDE: GIANT has only one parameter  $q$ , DANE has 4 parameters, and AIDE has 5 parameters.

**Datasets.** We conduct experiments on three real-world datasets—covtype ( $n = 581,012$  and  $d = 54$ ), w8a ( $n = 49,749$  and  $d = 300$ ), and a9a ( $n = 32,561$  and  $d = 123$ )—and their 1000-dimensional random Fourier features. We repeat experiments ten times; we report convergence curves of the 10 repeats as thin lines and their medians as thick lines. The results on different datasets are in Figures 9, 10, and 11.

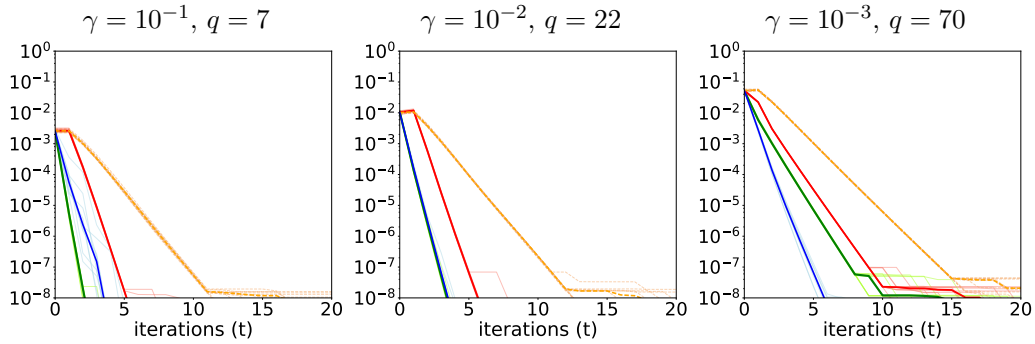
**Comparisons.** In terms of communications and epochs, DANE and GIANT have comparable convergence. GIANT works better when the condition number is large; DANE works better otherwise. This is essentially due to their local solvers: CG works better than SVRG when the condition number is large, and vice versa.

Nevertheless, in practice, GIANT can be a more practical choice than the alternatives as it involves much less parameter-tunings. More specifically, besides their common parameter

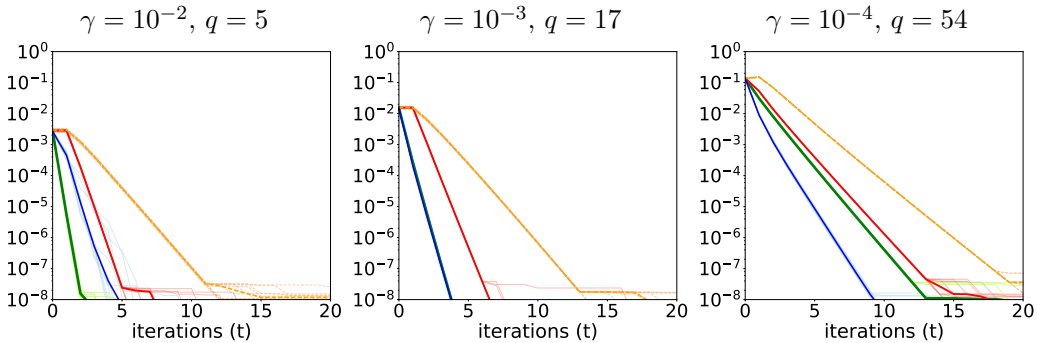
---

9. Two epochs for computing the full gradient; 10 epochs for line search;  $2q$  iterations for solving a local problem using CG or SVRG.

10. Here we cheat a bit because  $\kappa$  is unknown beforehand. In practice, it is unnecessary to know  $\kappa$ ; an arbitrary setting of  $q$ , as long as it is big, will make the compared methods converge rapidly. In addition, large or small  $q$  has the same effect on all the compared methods.



(a) Experiments on the 123-dimensional raw input. For the three settings of  $\gamma$ , the condition numbers of  $\mathbf{H}^*$  are respectively 12.2, 88.7, and 762.1.



(b) Experiments on the 1000-dimensional random Fourier features. For the three settings of  $\gamma$ , the condition numbers of  $\mathbf{H}^*$  are respectively 8.0, 55.1, and 450.2.

— GIANT    — DANE    — AIDE ( $\tau = 0.1$ )    - - - AIDE ( $\tau = 1$ )

Figure 11: Logistic regression on the a9a data and its random Fourier features. The  $x$ -axis is number of iterations; the  $y$ -axis is the ratio  $\frac{\|\mathbf{w}_t - \mathbf{w}^*\|_2}{\|\mathbf{w}^*\|_2}$ . The  $n = 32,561$  are randomly split to  $m = 16$  machines, and each machine holds  $s = \frac{n}{m} = 2035$  samples.  $\tau$  is the parameter of AIDE.

$q$  (iteration of local solvers), DANE and AIDE require fine-tuning of a few more parameters. In our experiments, we choose  $\eta_1$  from  $\{0.5, 1\}$  and the learning rate of SVRG from  $\{0.1, 1, 10\}$  and report the best result. However, we observe that DANE and AIDE are highly sensitive to learning rates: small learning rate leads to slow convergence, and large one leads to divergence. Since appropriate learning rate is *a priori unknown*, often many trials and errors are required to fine-tune the step-size. As a consequence, training procedure may incur additional computational efforts, most of which practically wasted, involving such parameter-tuning. For example, since we run DANE and AIDE six times to determine the two parameters, the actual computational cost of DANE is six times larger than what is reported in Figures 9, 10, and 11. If we take such additional computational costs into account, GIANT will be substantially more efficient than DANE and AIDE.

## 6. Conclusions and Future Works

We have proposed GIANT, a sound and highly practical Newton-type method, for empirical risk minimization in distributed computing environments. In comparison to similar methods, GIANT has three main advantageous features. First, GIANT is guaranteed to converge to high precisions in small number of iterations, provided that the number of training samples,  $n$ , is sufficiently large, relative to  $dm$ , where  $d$  is the number of features and  $m$  is the number of partitions. Second, GIANT is very communication efficient in that each iteration requires at most six rounds of communications, each with a complexity of merely  $\mathcal{O}(d \log m)$ . Third, in contrast to all other alternates, GIANT is easy to use, as it involves tuning of at most one hyper-parameter. Empirical studies have verified our theories and showcased the advantages of GIANT over other alternatives, namely DANE and AIDE.

For arbitrary loss functions, we only provided local convergence results, and thus required (rather pessimistically) that GIANT is initialize closed enough to the optimal solution. Following (Roosta-Khorasani and Mahoney, 2016a) and using a line-search globalization scheme, it is possible to obtain a globally convergent variant of GIANT. However, it is known that Newton-type methods using line-search suffer from a worst-case convergence rate which is worse than that of gradient descent. This is despite the widely observed fact that Newton-type methods almost always empirically outperform all variants of first-order methods, in terms of number of iterations required to achieve convergence. Improving such worst-case global convergence rate that can match that of the (accelerated) gradient method is yet an open problem and is worth studying.

GIANT works only for unconstrained problems with smooth and strongly convex objective function. GIANT can be naturally extended to *projected Newton* for constrained problems and *proximal Newton* for non-smooth regularizations, and weak convergence bounds can be easily established. However, strong convergence rates that match this work is nontrivial and unknown to us. Besides, the extension of GIANT to the trust-region methods may also be an interesting direction for future research.

## Appendix A. Implementation of GIANT

To implement Algorithm 1, it suffices to instantiate  $\mathbf{A}_t$  and  $\mathbf{b}_t$  defined in (6) and (7). We derive  $\mathbf{A}_t$  and  $\mathbf{b}_t$  for linear regression and logistic regression.

### A.1 Linear Regression

Let  $\mathbf{X} \in \mathbb{R}^{n \times d}$  be the feature matrix and  $\mathbf{y} \in \mathbb{R}^n$  the the response vector. We consider linear regression with any regularization  $r(\cdot)$ :

$$\min_{\mathbf{w} \in \mathbb{R}^d} \left\{ f(\mathbf{w}) \triangleq \frac{1}{2} \|\mathbf{X}\mathbf{w} - \mathbf{y}\|_2^2 + r(\mathbf{w}) \right\}.$$

The loss function is  $l_j(z) = \frac{1}{2}(z - y_j)^2$ . Its first and second-order derivatives are respectively  $l'_j(z) = z - y_j$  and  $l''_j(z) = 1$ . Then  $\mathbf{A}_t$  in (6) and  $\mathbf{b}_t$  in (7) can be respectively written as

$$\mathbf{A}_t = \frac{1}{\sqrt{n}} \mathbf{X} \in \mathbb{R}^{n \times d} \quad \text{and} \quad \mathbf{b}_t = \frac{1}{\sqrt{n}} (\mathbf{X}\mathbf{w}_t - \mathbf{y}) \in \mathbb{R}^n.$$

## A.2 Logistic Regression

Let  $\mathbf{y} \in \{-1, +1\}^n$  be the response vector. To make the derivation simpler, we apply each entry of  $\mathbf{y}$  to the corresponding feature vector; we denote  $\mathbf{x}_j$  as the product of  $y_j$  and the  $j$ -th feature vector. We consider logistic regression with any regularization  $r(\cdot)$ :

$$\min_{\mathbf{w} \in \mathbb{R}^d} \left\{ f(\mathbf{w}) \triangleq \frac{1}{n} \sum_{j=1}^n \log(1 + e^{-\mathbf{x}_j^T \mathbf{w}}) + r(\mathbf{w}) \right\}.$$

The loss function is  $l_j(z) = \log(1 + e^{-z})$ . Its first and second-order derivatives are respectively  $l'_j(z) = -\frac{1}{1+e^z}$  and  $l''_j(z) = \frac{e^z}{(1+e^z)^2}$ . Let

$$\begin{aligned} \mathbf{c}_t &= \left[ l'_1(\mathbf{x}_1^T \mathbf{w}), \dots, l'_n(\mathbf{x}_n^T \mathbf{w}) \right]^T = - \left[ \frac{1}{1+\exp(\mathbf{x}_1^T \mathbf{w}_t)}, \dots, \frac{1}{1+\exp(\mathbf{x}_n^T \mathbf{w}_t)} \right]^T, \\ \mathbf{D}_t &= \text{diag} \left[ \sqrt{l''_1(\mathbf{x}_1^T \mathbf{w})}, \dots, \sqrt{l''_n(\mathbf{x}_n^T \mathbf{w})} \right]^T = \text{diag} \left[ \frac{\exp(\mathbf{x}_1^T \mathbf{w}_t/2)}{1+\exp(\mathbf{x}_1^T \mathbf{w}_t)}, \dots, \frac{\exp(\mathbf{x}_n^T \mathbf{w}_t/2)}{1+\exp(\mathbf{x}_n^T \mathbf{w}_t)} \right]^T. \end{aligned}$$

Then  $\mathbf{A}_t$  in (6) and  $\mathbf{b}_t$  in (7) can be respectively written as

$$\mathbf{A}_t = \frac{1}{\sqrt{n}} \mathbf{D}_t \mathbf{X} \in \mathbb{R}^{n \times d} \quad \text{and} \quad \mathbf{b}_t = \frac{1}{\sqrt{n}} \mathbf{D}_t^{-1} \mathbf{c}_t \in \mathbb{R}^n.$$

## Appendix B. Descriptions of Compared Work

In the experiments of logistic regression, we compare with DANE and AIDE. Here we describe the implementation of the two methods.

### B.1 DANE

Let the objective function  $f(\mathbf{w}) = \frac{1}{n} \sum_{i=1}^n f_i(\mathbf{w})$  be defined in (1). The Distributed Approximate NEwton-type method (DANE) (Shamir et al., 2014) iteratively updates  $\mathbf{w}$  by

$$\mathbf{w}_{t+1,i} = \underset{\mathbf{w}}{\text{argmin}} \left\{ \frac{1}{s} \sum_{j \in \mathcal{J}'_i} \left( f_j(\mathbf{w}) - \langle \nabla f_j(\mathbf{w}_t) - \eta_1 \nabla f(\mathbf{w}_t), \mathbf{w} \rangle \right) + \frac{\eta_2}{2} \|\mathbf{w} - \mathbf{w}_t\|_2^2 \right\} \quad (17)$$

for all  $i \in [m]$  and  $\mathbf{w}_{t+1} = \frac{1}{m} \sum_{i=1}^m \mathbf{w}_{t+1,i}$ . Here  $\eta_1$  and  $\eta_2$  are some user-specified positive parameters.

**Solving the local problems.** The local problem (17) can be solved by many off-the-shelf numerical algorithms. If  $f$  is non-quadratic, exact solution to (17) is not generally attainable. Reddi et al. (2016) proposed to solve (17) inexactly by SVRG (Johnson and Zhang, 2013) and call the method *inexact DANE*. We will simply refer to the inexact DANE as DANE. To solve the logistic regression problem, we tried mini-batch SVRG with batch size 100, which is a variant of SVRG, and gradient descent with momentum; it turned out that SVRG converges much faster in terms of epochs. Note that SVRG has three parameters: (1) the maximum iterations (or some other stopping criteria) of the outer loop, (2) the learning rate (a.k.a. step size), and (3) the maximum iterations of the inner loop. The performance of SVRG is sensitive to the first two parameters but insensitive to the third; we tune the first two and simply let the inner loop go one pass through the local data.

**Tuning parameters.** To summarize, DANE has totally four tuning parameters: two explicit parameters in (17) and two implicit tuning parameters in SVRG.

**Relation to GIANT.** If  $\eta_1 = 1$  and  $\eta_2 = 0$  and the loss function is quadratic, then DANE and our method are identical. For non-quadratic loss, DANE and GIANT are different but have strong resemblance. In (17), if  $f_j$  is replaced by its quadratic approximation, then DANE becomes GIANT.

## B.2 AIDE

Let  $f_{t,j}(\mathbf{w}) = f_j(\mathbf{w}) + \frac{\tau}{2}\|\mathbf{w} - \mathbf{z}_t\|_2^2$  and  $f_t(\mathbf{w}) = \frac{1}{n}f_{t,j}(\mathbf{w})$ , where  $\mathbf{z}_t = \mathbf{w}_t + \beta_t(\mathbf{w}_t - \mathbf{w}_{t-1})$  for some  $\beta_t \in (0, 1)$  which is self-tuned. AIDE updates  $\mathbf{w}$  by

$$\mathbf{w}_{t+1,j} = \underset{\mathbf{w}}{\operatorname{argmin}} \left\{ \frac{1}{s} \sum_{j \in \mathcal{J}'_i} \left( f_{t,j}(\mathbf{w}) - \langle \nabla f_{t,j}(\mathbf{w}_t) - \eta_1 \nabla f_t(\mathbf{w}_t), \mathbf{w} \rangle \right) + \frac{\eta_2}{2} \|\mathbf{w} - \mathbf{w}_t\|_2^2 \right\}$$

for all  $i \in [m]$  and  $\mathbf{w}_{t+1} = \frac{1}{m} \sum_{i=1}^m \mathbf{w}_{t+1,i}$ . AIDE enjoys global convergence, and its required number of iterations has square root dependence on the condition number of  $f$ . Their theory does not indicate the benefit of large local sample size  $s$ .

**Tuning parameters.** AIDE has totally five tuning parameters. AIDE invokes DANE as its subroutine, so AIDE has all the four tuning parameters of DANE. Besides, AIDE has the additional tuning parameter  $\tau$ .

## Appendix C. Proof of the Main Results

In this section prove the main results: Theorems 1, 2, 4 and Corollary 3. In Section C.1 we first define the notation used throughout. In Sections C.2 to C.4 we establish or cite several lemmas which are applied to prove our main theorems. Lemmas 7, 8, and 10 are new and may have independent interest beyond the scope of this paper. In Section C.5 we complete the proof of the main theorems and corollaries.

### C.1 Notation

Let  $\mathbf{A}_t$  and  $\mathbf{b}_t$  be respectively defined in (6) and (7). Let  $\mathbf{c}_t = \mathbf{b}_t + (\mathbf{A}_t^T)^\dagger \mathbf{M} \mathbf{w}_t$ . We define the auxiliary function

$$\phi_t(\mathbf{p}) \triangleq \frac{1}{2} \mathbf{p}^T \underbrace{(\mathbf{A}_t^T \mathbf{A}_t + \mathbf{M})}_{\mathbf{H}_t} \mathbf{p} - \mathbf{p}^T \underbrace{\mathbf{A}_t^T \mathbf{c}_t}_{\mathbf{g}_t} \quad (18)$$

and study its approximate solutions in this section. The Newton direction at  $\mathbf{w}_t$  can be written as

$$\mathbf{p}_t^* = \underset{\mathbf{p}}{\operatorname{argmin}} \phi_t(\mathbf{p}) = (\mathbf{A}_t^T \mathbf{A}_t + \mathbf{M})^{-1} \mathbf{A}_t^T \mathbf{c}_t.$$

Let  $\mathbf{S}_1, \dots, \mathbf{S}_m$  be some sketching matrices. By definition, the local and global approximate Newton directions are respectively

$$\tilde{\mathbf{p}}_{t,i} = (\mathbf{A}_t^T \mathbf{S}_i \mathbf{S}_i^T \mathbf{A}_t + \mathbf{M})^{-1} \mathbf{A}_t^T \mathbf{c}_t \quad \text{and} \quad \tilde{\mathbf{p}}_t = \frac{1}{m} \sum_{i=1}^m \tilde{\mathbf{p}}_{t,i}. \quad (19)$$

It can be verified that  $\tilde{\mathbf{p}}_{t,i}$  is the minimizer of the sketched problem

$$\tilde{\phi}_{t,i}(\mathbf{p}) \triangleq \frac{1}{2} \mathbf{p}^T \underbrace{(\mathbf{A}_t^T \mathbf{S}_i \mathbf{S}_i^T \mathbf{A}_t + \mathbf{M})}_{\tilde{\mathbf{H}}_{t,i}} \mathbf{p} - \mathbf{p}^T \underbrace{\mathbf{A}_t^T \mathbf{c}_t}_{\mathbf{g}_t}. \quad (20)$$

We will show that  $\tilde{\mathbf{p}}_t$  is close to  $\mathbf{p}_t^*$  in terms of the value of the function  $\phi_t(\cdot)$ . This is the key to the convergence analysis of GIANT.

## C.2 Analysis of Model Averaging

Lemma 7 shows that  $\phi_t(\tilde{\mathbf{p}}_t)$  is close to  $\phi_t(\mathbf{p}_t^*)$ . Note that  $\phi_t(\tilde{\mathbf{p}}_t)$  and  $\phi_t(\mathbf{p}_t^*)$  are both non-positive. The proof of Lemma 7 uses some techniques developed by Wang et al. (2017). We prove Lemma 7 in Appendix D.

**Assumption 3** Let  $\epsilon \in (0, 1)$  be any fixed parameter,  $\rho = \text{rank}(\mathbf{A}_t)$ , and  $\mathbf{U} \in \mathbb{R}^{n \times \rho}$  be the orthogonal bases of  $\mathbf{A}_t$ . Let  $\mathbf{S}_1, \dots, \mathbf{S}_m \in \mathbb{R}^{n \times s}$  be certain sketching matrices and  $\mathbf{S} = \frac{1}{\sqrt{m}}[\mathbf{S}_1, \dots, \mathbf{S}_m] \in \mathbb{R}^{n \times ms}$ ; here  $s$  depends on  $\epsilon$ . Assume  $\mathbf{S}_i$  and  $\mathbf{S}$  satisfy

$$\|\mathbf{U}^T \mathbf{S}_i \mathbf{S}_i^T \mathbf{U} - \mathbf{I}_\rho\|_2 \leq \epsilon \quad \text{for all } i \in [m] \quad \text{and} \quad \|\mathbf{U}^T \mathbf{S} \mathbf{S}^T \mathbf{U} - \mathbf{I}_\rho\|_2 \leq \frac{\epsilon}{m}.$$

**Lemma 7 (Exact Solution to Subproblems)** Let  $\mathbf{S}_1, \dots, \mathbf{S}_m \in \mathbb{R}^{n \times s}$  satisfy Assumption 3. Let  $\phi_t$  be defined in (18) and  $\tilde{\mathbf{p}}_t$  be defined in (19). It holds that

$$\min_{\mathbf{p}} \phi_t(\mathbf{p}) \leq \phi_t(\tilde{\mathbf{p}}_t) \leq (1 - \alpha^2) \cdot \min_{\mathbf{p}} \phi_t(\mathbf{p}),$$

where  $\alpha = \vartheta \left( \frac{\epsilon}{m} + \frac{\epsilon^2}{1-\epsilon} \right)$  and  $\vartheta = \frac{\sigma_{\max}(\mathbf{A}_t^T \mathbf{A}_t)}{\sigma_{\max}(\mathbf{A}_t^T \mathbf{A}_t) + \sigma_{\min}(\mathbf{M})} \leq 1$ .

Lemma 7 requires the exact minimizer to  $\tilde{\phi}_{t,i}(\cdot)$  in (20), denote  $\tilde{\mathbf{p}}_{t,i}$ , which requires the computation of  $\tilde{\mathbf{H}}_{t,i} = \mathbf{A}_t^T \mathbf{S}_i \mathbf{S}_i^T \mathbf{A}_t + \mathbf{M}$  and its inversion. Alternatively, we can use numerical optimization, such as CG, to optimize  $\tilde{\phi}_{t,i}(\cdot)$  up to a fixed precision. We denote the inexact solution as  $\tilde{\mathbf{p}}'_{t,i}$  and assume it is close to the exact solution  $\tilde{\mathbf{p}}_{t,i}$ . Then  $\tilde{\mathbf{p}}'_{t,i}$  is also a good approximation to  $\mathbf{p}_t^*$  in terms of the values of  $\phi_t(\cdot)$ . We prove Lemma 8 in Appendix E.

**Lemma 8 (Inexact Solution to Subproblems)** Let  $\mathbf{S}_1, \dots, \mathbf{S}_m \in \mathbb{R}^{n \times s}$  satisfy Assumption 3. Let  $\tilde{\mathbf{p}}_{t,i}$  and  $\tilde{\mathbf{H}}_{t,i}$  be defined in (19) and (20), respectively. Let  $\tilde{\mathbf{p}}'_{t,i}$  be any vector satisfying

$$\left\| \tilde{\mathbf{H}}_{t,i}^{1/2} (\tilde{\mathbf{p}}'_{t,i} - \tilde{\mathbf{p}}_{t,i}) \right\|_2 \leq \epsilon_0 \left\| \tilde{\mathbf{H}}_{t,i}^{1/2} \tilde{\mathbf{p}}_{t,i} \right\|_2$$

for some fixed  $\epsilon_0 \in (0, 1)$ . Let  $\tilde{\mathbf{p}}'_t = \frac{1}{m} \sum_{i=1}^m \tilde{\mathbf{p}}'_{t,i}$ . Let  $\phi_t$  be defined in (18). It holds that

$$\min_{\mathbf{p}} \phi_t(\mathbf{p}) \leq \phi_t(\tilde{\mathbf{p}}'_t) \leq (1 - \alpha'^2) \cdot \min_{\mathbf{p}} \phi_t(\mathbf{p}),$$

where  $\alpha' = \vartheta \left( \frac{\epsilon}{m} + \frac{\epsilon^2}{1-\epsilon} \right) + \frac{\epsilon_0}{1-\epsilon}$  and  $\vartheta = \frac{\sigma_{\max}^2(\mathbf{A}_t)}{\sigma_{\max}^2(\mathbf{A}_t) + \sigma_{\min}(\mathbf{M})} \leq 1$ .

### C.3 Analysis of Uniform Sampling

Lemma 7 and 8 require the sketching matrices satisfying some properties. Lemma 9, which is cited from (Wang et al., 2017), shows that uniform sampling matrices enjoys the properties in Assumption 3 for an appropriately-chosen sample size  $s$ . The proof of Lemma 9 is based on the results in (Drineas et al., 2006b, 2011, Woodruff, 2014, Wang et al., 2016).

**Lemma 9** *Let  $\epsilon, \delta \in (0, 1)$  be fixed parameters. Let  $\mathbf{U} \in \mathbb{R}^{n \times \rho}$  be any fixed matrix with orthonormal columns. Let  $\mathbf{S}_1, \dots, \mathbf{S}_m \in \mathbb{R}^{n \times s}$  be independent uniform sampling matrices with  $s = \Theta(\frac{\mu \rho}{\epsilon^2} \log \frac{\rho m}{\delta})$  and  $\mathbf{S} \in \mathbb{R}^{n \times ms}$  be the concatenation of  $\mathbf{S}_1, \dots, \mathbf{S}_m$ . It holds with probability at least  $1 - \delta$  that*

$$\|\mathbf{U}^T \mathbf{S}_i \mathbf{S}_i^T \mathbf{U} - \mathbf{I}_\rho\|_2 \leq \epsilon \quad \text{for all } i \in [m] \quad \text{and} \quad \|\mathbf{U}^T \mathbf{S} \mathbf{S}^T \mathbf{U} - \mathbf{I}_\rho\|_2 \leq \frac{\epsilon}{m}.$$

Besides uniform sampling, other sketching methods such as leverage score sampling (Drineas et al., 2006b), Gaussian projection (Johnson and Lindenstrauss, 1984), Rademacher random variables (Achlioptas, 2003), subsampled randomized Hadamard transform (Tropp, 2011, Drineas et al., 2011, Lu et al., 2013) also satisfy Assumption 3. In addition, these sketching methods eliminate the dependence of  $s$  on the matrix coherence  $\mu$ . These sketches are more expensive to implement than simple uniform sampling (e.g., to compute approximations to the leverage scores with the algorithm of Drineas et al. (2012) takes roughly the amount of time it takes to implement a random projection), and an obvious question raised by our results is whether there exists a point in communication-computation tradeoff space where using these sketches would be better than performing simple uniform sampling.

### C.4 Analysis of the Approximate Newton Step

Let  $\phi_t$  be defined in (18); note that  $\phi_t$  is non-positive. If the approximate Newton direction  $\tilde{\mathbf{p}}_t$  is close to the exact Newton step  $\mathbf{p}_t^*$  in terms of  $\phi_t$ , then  $\tilde{\mathbf{p}}$  is provably a good descending direction. The proof follows the classical local convergence analysis of Newton's method (Wright and Nocedal, 1999). We prove Lemma 10 in Appendix F.

**Lemma 10** *Assume the Hessian matrix is  $L$ -Lipschitz at  $\mathbf{w}^*$ :  $\|\mathbf{H}(\mathbf{w}_t) - \mathbf{H}(\mathbf{w}^*)\|_2 \leq L\|\mathbf{w}_t - \mathbf{w}^*\|_2$ . Let  $\alpha \in (0, 1)$  be any fixed error parameter. Assume  $\tilde{\mathbf{p}}_t$  satisfy*

$$\phi_t(\tilde{\mathbf{p}}_t) \leq (1 - \alpha^2) \cdot \min_{\mathbf{p}} \phi_t(\mathbf{p}).$$

*Then  $\Delta_t = \mathbf{w}_t - \mathbf{w}^*$  satisfies*

$$\Delta_{t+1}^T \mathbf{H}_t \Delta_{t+1} \leq L \|\Delta_t\|_2^2 \|\Delta_{t+1}\|_2 + \frac{\alpha^2}{1 - \alpha^2} \Delta_t^T \mathbf{H}_t \Delta_t.$$

### C.5 Completing the Proofs

Finally, we prove our main results using the lemmas in this section. Let  $\mu_t$  be the row coherence of  $\mathbf{A}_t$  and  $s = \Theta(\frac{\mu_t d}{\epsilon^2} \log \frac{dm}{\delta})$ . Let  $\alpha = \frac{\epsilon}{m} + \frac{\epsilon^2}{1 - \epsilon}$ ,  $L$  be defined in Lemma 10, and  $\Delta_t = \mathbf{w}_t - \mathbf{w}^*$ . It follows from Lemma 9 that uniform sampling matrices satisfy Assumption 3 with probability (w.p.) at least  $1 - \delta$ . It follows from Lemmas 7 and 10 that

$$\Delta_{t+1}^T \mathbf{H}_t \Delta_{t+1} \leq L \|\Delta_t\|_2^2 \|\Delta_{t+1}\|_2 + \frac{\alpha^2}{1 - \alpha^2} \Delta_t^T \mathbf{H}_t \Delta_t \quad (21)$$

holds w.p.  $1 - \delta$ .

**Proof of Theorem 1.** If the loss function is quadratic, then  $\mathbf{H}(\mathbf{w}_0) = \mathbf{H}(\mathbf{w}_1) = \dots = \mathbf{H}(\mathbf{w}^*)$ ; obviously,  $\mathbf{H}(\mathbf{w})$  is 0-Lipschitz. Thus we let  $\mathbf{H} \triangleq \mathbf{H}(\mathbf{w})$  for all  $\mathbf{w}$ . It follows from (21) that w.p.  $1 - \delta$ ,

$$\Delta_{t+1}^T \mathbf{H} \Delta_{t+1} \leq \frac{\alpha^2}{1-\alpha^2} \Delta_t^T \mathbf{H} \Delta_t \leq \left(\frac{\alpha^2}{1-\alpha^2}\right)^{t+1} \Delta_0^T \mathbf{H} \Delta_0.$$

It follows that w.p.  $1 - \delta$ ,

$$\frac{\|\Delta_t\|_2}{\|\Delta_0\|_2} \leq \left(\frac{\alpha}{\sqrt{1-\alpha^2}}\right)^t \sqrt{\frac{\sigma_{\max}(\mathbf{H})}{\sigma_{\min}(\mathbf{H})}}. \quad (22)$$

**Proof of Theorem 2.** It follows from (21) that w.p.  $1 - \delta$ ,

$$\Delta_{t+1}^T \mathbf{H}_t \Delta_{t+1} \leq \max \left\{ 2L \|\Delta_t\|_2^2 \|\Delta_{t+1}\|_2, \frac{2\alpha^2}{1-\alpha^2} \Delta_t^T \mathbf{H}_t \Delta_t \right\}.$$

It follows that w.p.  $1 - \delta$ , at least one of the following two inequalities hold:

$$\begin{aligned} \|\Delta_{t+1}\|_2 &\leq \frac{2L}{\sigma_{\min}(\mathbf{H}_t)} \|\Delta_t\|_2^2, \\ \|\Delta_{t+1}\|_2 &\leq \frac{\alpha}{\sqrt{1-\alpha^2}} \sqrt{\frac{2\sigma_{\max}(\mathbf{H}_t)}{\sigma_{\min}(\mathbf{H}_t)}} \|\Delta_t\|_2, \end{aligned} \quad (23)$$

which proves Theorem 2.

**Proof of Corollary 3.** Under Assumptions 1, it holds that  $\|\mathbf{H}_t - \mathbf{H}^*\|_2 \leq L \|\Delta_t\|_2$ . It follows that

$$\sigma_{\min}(\mathbf{H}^*) - L \|\Delta_t\|_2 \leq \sigma_{\min}(\mathbf{H}_t) \leq \sigma_{\max}(\mathbf{H}_t) \leq \sigma_{\max}(\mathbf{H}^*) + L \|\Delta_t\|_2.$$

It follows from Assumption 2 that

$$\begin{aligned} \frac{\sigma_{\max}(\mathbf{H}_t)}{\sigma_{\min}(\mathbf{H}_t)} &\leq \frac{\sigma_{\max}(\mathbf{H}^*) + L \|\Delta_t\|_2}{\sigma_{\min}(\mathbf{H}^*) - L \|\Delta_t\|_2} \leq 2 \frac{\sigma_{\max}(\mathbf{H}^*)}{\sigma_{\min}(\mathbf{H}^*)}, \\ \frac{L}{\sigma_{\min}(\mathbf{H}_t)} &\leq \frac{L}{\sigma_{\min}(\mathbf{H}^*) - L \|\Delta_t\|_2} \leq \frac{3}{2} \frac{L}{\sigma_{\min}(\mathbf{H}^*)}. \end{aligned}$$

It follows from (23) that

$$\begin{aligned} \|\Delta_{t+1}\|_2 &\leq \max \left\{ \alpha \sqrt{\frac{2\sigma_{\max}(\mathbf{H}_t)}{\sigma_{\min}(\mathbf{H}_t)}} \|\Delta_t\|_2, \frac{2L}{\sigma_{\min}(\mathbf{H}_t)} \|\Delta_t\|_2^2 \right\} \\ &\leq \max \left\{ 2\alpha \sqrt{\frac{\sigma_{\max}(\mathbf{H}^*)}{\sigma_{\min}(\mathbf{H}^*)}} \|\Delta_t\|_2, \frac{3L}{\sigma_{\min}(\mathbf{H}^*)} \|\Delta_t\|_2^2 \right\} \end{aligned}$$

holds with probability at least  $1 - \delta$ .

**Proof of Theorem 4.** In the proof of (21), we replace Lemma 7 by Lemma 8 and  $\alpha$  by  $\alpha'$ . Then very similar results can be proved in the same way as Theorems 1 and 2 and Corollary 3.

**Proof of Corollary 5.** Let  $\mathbf{p}_0$  be an arbitrary initialization. Standard convergence bound of CG (Golub and Van Loan, 2012) guarantees that

$$\frac{\|\tilde{\mathbf{H}}_{t,i}^{1/2}(\tilde{\mathbf{p}}'_{t,i} - \tilde{\mathbf{p}}_{t,i})\|_2^2}{\|\tilde{\mathbf{H}}_{t,i}^{1/2}(\mathbf{p}_0 - \tilde{\mathbf{p}}_{t,i})\|_2^2} \leq 2\left(\frac{\sqrt{\tilde{\kappa}_t} - 1}{\sqrt{\tilde{\kappa}_t} + 1}\right)^q,$$

where  $\tilde{\kappa}_t$  is the condition number of  $\tilde{\mathbf{H}}_{t,i}$ . Let the righthand-side equal to  $\frac{\epsilon_0^2}{4}$ . It follows that  $q = \log \frac{8}{\epsilon_0^2} / \log \frac{\sqrt{\tilde{\kappa}_t} + 1}{\sqrt{\tilde{\kappa}_t} - 1}$ . Then (12) follows by letting  $\mathbf{p}_0 = \mathbf{0}$ . Because  $(1 - \epsilon)\mathbf{H}_t \preceq \tilde{\mathbf{H}}_{t,i} \preceq (1 + \epsilon)\mathbf{H}_t$ , their condition numbers satisfy

$$\frac{1-\epsilon}{1+\epsilon}\kappa(\mathbf{H}_t) \leq \tilde{\kappa}_t \leq \frac{1+\epsilon}{1-\epsilon}\kappa(\mathbf{H}_t).$$

Clearly,  $\tilde{\kappa}_t$  is very close to  $\kappa_t \triangleq \kappa(\mathbf{H}_t)$ .

#### Appendix D. Proof of Lemma 7 (Model Averaging)

We use the notation in Appendix C.1. Here we leave out the subscript  $t$ . By the definitions of  $\tilde{\mathbf{p}}_i$  and  $\mathbf{p}^*$ , we have that

$$\begin{aligned} (\mathbf{A}^T \mathbf{A} + \mathbf{M})^{1/2}(\tilde{\mathbf{p}}_i - \mathbf{p}^*) &= (\mathbf{A}^T \mathbf{A} + \mathbf{M})^{1/2}[(\mathbf{A}^T \mathbf{S}_i \mathbf{S}_i^T \mathbf{A} + \mathbf{M})^{-1} - (\mathbf{A}^T \mathbf{A} + \mathbf{M})^{-1}] \mathbf{A}^T \mathbf{c} \\ &= (\mathbf{A}^T \mathbf{A} + \mathbf{M})^{1/2}(\mathbf{A}^T \mathbf{A} + \mathbf{M})^{-1}(\mathbf{A}^T \mathbf{A} + \mathbf{M} - \mathbf{A}^T \mathbf{S}_i \mathbf{S}_i^T \mathbf{A} - \mathbf{M})(\mathbf{A}^T \mathbf{S}_i \mathbf{S}_i^T \mathbf{A} + \mathbf{M})^{-1} \mathbf{A}^T \mathbf{c} \\ &= (\mathbf{A}^T \mathbf{A} + \mathbf{M})^{-1/2}(\mathbf{A}^T \mathbf{A} - \mathbf{A}^T \mathbf{S}_i \mathbf{S}_i^T \mathbf{A})(\mathbf{A}^T \mathbf{S}_i \mathbf{S}_i^T \mathbf{A} + \mathbf{M})^{-1} \mathbf{A}^T \mathbf{c}, \end{aligned}$$

where the second equality follows from that  $\mathbf{R}^{-1} - \mathbf{T}^{-1} = \mathbf{T}^{-1}(\mathbf{T} - \mathbf{R})\mathbf{R}^{-1}$  for nonsingular matrices  $\mathbf{R}$  and  $\mathbf{T}$ . We define

$$(\mathbf{A}^T \mathbf{A} + \mathbf{M})^{1/2}(\tilde{\mathbf{p}}_i - \mathbf{p}^*) = \mathbf{\Gamma}_i \mathbf{K}_i \mathbf{r}, \quad (24)$$

where

$$\begin{aligned} \mathbf{\Gamma}_i &= (\mathbf{A}^T \mathbf{A} + \mathbf{M})^{-1/2}(\mathbf{A}^T \mathbf{A} - \mathbf{A}^T \mathbf{S}_i \mathbf{S}_i^T \mathbf{A})(\mathbf{A}^T \mathbf{A} + \mathbf{M})^{-1/2}, \\ \mathbf{K}_i &= (\mathbf{A}^T \mathbf{A} + \mathbf{M})^{1/2}(\mathbf{A}^T \mathbf{S}_i \mathbf{S}_i^T \mathbf{A} + \mathbf{M})^{-1}(\mathbf{A}^T \mathbf{A} + \mathbf{M})^{1/2}, \\ \mathbf{r} &= (\mathbf{A}^T \mathbf{A} + \mathbf{M})^{-1/2} \mathbf{A}^T \mathbf{c}. \end{aligned}$$

By Assumption 3, we have  $(1 - \epsilon)\mathbf{A}^T \mathbf{A} \preceq \mathbf{A}^T \mathbf{S}_i \mathbf{S}_i^T \mathbf{A} \preceq (1 + \epsilon)\mathbf{A}^T \mathbf{A}$ . It follows that

$$(1 - \epsilon)(\mathbf{A}^T \mathbf{A} + \mathbf{M}) \preceq (\mathbf{A}^T \mathbf{S}_i \mathbf{S}_i^T \mathbf{A} + \mathbf{M}) \preceq (1 + \epsilon)(\mathbf{A}^T \mathbf{A} + \mathbf{M}),$$

and thus  $\frac{1}{1+\epsilon}\mathbf{I}_d \preceq \mathbf{K}_i \preceq \frac{1}{1-\epsilon}\mathbf{I}_d$ . Let  $\mathbf{K}_i = \mathbf{I}_d + \mathbf{\Upsilon}_i$ . It holds that

$$-\frac{\epsilon}{1+\epsilon}\mathbf{I}_d \preceq \mathbf{\Upsilon}_i \preceq \frac{\epsilon}{1-\epsilon}\mathbf{I}_d. \quad (25)$$

It follows from (24) that

$$\begin{aligned} (\mathbf{A}^T \mathbf{A} + \mathbf{M})^{1/2}(\tilde{\mathbf{p}} - \mathbf{p}^*) &= \frac{1}{m} \sum_{i=1}^m (\mathbf{A}^T \mathbf{A} + \mathbf{M})^{1/2}(\tilde{\mathbf{p}}_i - \mathbf{p}^*) \\ &= \frac{1}{m} \sum_{i=1}^m \mathbf{\Gamma}_i \mathbf{K}_i \mathbf{r} = \frac{1}{m} \sum_{i=1}^m \mathbf{\Gamma}_i \mathbf{r} + \frac{1}{m} \sum_{i=1}^m \mathbf{\Gamma}_i \mathbf{\Upsilon}_i \mathbf{r}. \end{aligned} \quad (26)$$

It follows from Assumption 3 that

$$\begin{aligned}\|\Gamma_i\|_2 &\leq \epsilon \left\| (\mathbf{A}^T \mathbf{A} + \mathbf{M})^{-\frac{1}{2}} (\mathbf{A}^T \mathbf{A}) (\mathbf{A}^T \mathbf{A} + \mathbf{M})^{-\frac{1}{2}} \right\|_2, \\ \left\| \frac{1}{m} \sum_{i=1}^m \Gamma_i \right\|_2 &\leq \frac{\epsilon}{m} \left\| (\mathbf{A}^T \mathbf{A} + \mathbf{M})^{-\frac{1}{2}} (\mathbf{A}^T \mathbf{A}) (\mathbf{A}^T \mathbf{A} + \mathbf{M})^{-\frac{1}{2}} \right\|_2.\end{aligned}$$

Let  $\mathbf{A} = \mathbf{U}\Sigma\mathbf{V}$  be the thin SVD ( $\Sigma$  is  $d \times d$ ). It holds that

$$\begin{aligned}& (\mathbf{A}^T \mathbf{A} + \mathbf{M})^{-\frac{1}{2}} (\mathbf{A}^T \mathbf{A}) (\mathbf{A}^T \mathbf{A} + \mathbf{M})^{-\frac{1}{2}} \\ &= \mathbf{V}(\Sigma^2 + \mathbf{V}^T \mathbf{M} \mathbf{V})^{-1/2} \Sigma^2 (\Sigma^2 + \mathbf{V}^T \mathbf{M} \mathbf{V})^{-1/2} \mathbf{V}^T \\ &= \mathbf{V} \Sigma^{-1} [\Sigma(\Sigma^2 + \mathbf{V}^T \mathbf{M} \mathbf{V})^{-1/2} \Sigma]^2 \Sigma^{-1} \mathbf{V}^T \\ &\leq \mathbf{V} \Sigma^{-1} [\Sigma(\Sigma^2 + \sigma_{\min}(\mathbf{M})\mathbf{I}_\rho)^{-1/2} \Sigma]^2 \Sigma^{-1} \mathbf{V}^T \\ &= \mathbf{V} \Sigma^2 [\Sigma^2 + \sigma_{\min}(\mathbf{M})\mathbf{I}_\rho]^{-1} \mathbf{V}^T \preceq \frac{\sigma_{\max}(\mathbf{A}_t^T \mathbf{A}_t)}{\sigma_{\max}(\mathbf{A}_t^T \mathbf{A}_t) + \sigma_{\min}(\mathbf{M})} \mathbf{I}_d \triangleq \vartheta \mathbf{I}_d.\end{aligned}$$

It follows that

$$\|\Gamma_i\|_2 \leq \vartheta \epsilon \quad \text{and} \quad \left\| \frac{1}{m} \sum_{i=1}^m \Gamma_i \right\|_2 \leq \frac{\vartheta \epsilon}{m}. \quad (27)$$

It follows from (25), (26), (27) that

$$\begin{aligned}\left\| (\mathbf{A}^T \mathbf{A} + \mathbf{M})^{1/2} (\tilde{\mathbf{p}} - \mathbf{p}^*) \right\|_2 &\leq \left\| \frac{1}{m} \sum_{i=1}^m \Gamma_i \mathbf{r} \right\|_2 + \left\| \frac{1}{m} \sum_{i=1}^m \Gamma_i \Upsilon_i \mathbf{r} \right\|_2 \\ &\leq \frac{\vartheta \epsilon}{m} \|\mathbf{r}\|_2 + \frac{1}{m} \sum_{i=1}^m \vartheta \epsilon \|\Upsilon_i\|_2 \|\mathbf{r}\|_2 \leq \vartheta \left( \frac{\epsilon}{m} + \frac{\epsilon^2}{1-\epsilon} \right) \|\mathbf{r}\|_2 \\ &= \vartheta \left( \frac{\epsilon}{m} + \frac{\epsilon^2}{1-\epsilon} \right) \left\| (\mathbf{A}^T \mathbf{A} + \mathbf{M})^{-1/2} \mathbf{A}^T \mathbf{c} \right\|_2 = \vartheta \left( \frac{\epsilon}{m} + \frac{\epsilon^2}{1-\epsilon} \right) \left\| (\mathbf{A}^T \mathbf{A} + \mathbf{M})^{1/2} \mathbf{p}^* \right\|_2.\end{aligned} \quad (28)$$

By the definition of  $\phi(\mathbf{p})$  and  $\mathbf{p}^*$ , it can be shown that

$$\phi(\mathbf{p}^*) = -\left\| (\mathbf{A}^T \mathbf{A} + \mathbf{M})^{-1/2} \mathbf{A}^T \mathbf{c} \right\|_2^2 = -\left\| (\mathbf{A}^T \mathbf{A} + \mathbf{M})^{1/2} \mathbf{p}^* \right\|_2^2.$$

For any  $\mathbf{p} \in \mathbb{R}^d$ , it holds that

$$\begin{aligned}\phi(\mathbf{p}) - \phi(\mathbf{p}^*) &= \left\| (\mathbf{A}^T \mathbf{A} + \mathbf{M})^{1/2} \mathbf{p} \right\|_2^2 - 2\mathbf{c}^T \mathbf{A} \mathbf{p} + \left\| (\mathbf{A}^T \mathbf{A} + \mathbf{M})^{-1/2} \mathbf{A}^T \mathbf{c} \right\|_2^2 \\ &= \left\| (\mathbf{A}^T \mathbf{A} + \mathbf{M})^{1/2} \mathbf{p} - (\mathbf{A}^T \mathbf{A} + \mathbf{M})^{-1/2} \mathbf{A}^T \mathbf{c} \right\|_2^2 = \left\| (\mathbf{A}^T \mathbf{A} + \mathbf{M})^{1/2} (\mathbf{p} - \mathbf{p}^*) \right\|_2^2.\end{aligned} \quad (29)$$

It follows from (28) and (29) that

$$\begin{aligned}\phi(\tilde{\mathbf{p}}) - \phi(\mathbf{p}^*) &= \left\| (\mathbf{A}^T \mathbf{A} + \mathbf{M})^{1/2} (\tilde{\mathbf{p}} - \mathbf{p}^*) \right\|_2^2 \\ &\leq \vartheta^2 \left( \frac{\epsilon}{m} + \frac{\epsilon^2}{1-\epsilon} \right)^2 \left\| (\mathbf{A}^T \mathbf{A} + \mathbf{M})^{1/2} \mathbf{p}^* \right\|_2^2 = -\vartheta^2 \left( \frac{\epsilon}{m} + \frac{\epsilon^2}{1-\epsilon} \right)^2 \phi(\mathbf{p}^*),\end{aligned}$$

by which the lemma follows.

## Appendix E. Proof of Lemma 8 (Effect of Inexact Solution)

We use the notation in Appendix C.1. We leave out the subscript  $t$ . Let us first bound  $\|(\mathbf{A}^T \mathbf{A} + \mathbf{M})^{1/2}(\tilde{\mathbf{p}}'_i - \tilde{\mathbf{p}}_i)\|_2^2$ . By Assumption 3 and that  $\tilde{\mathbf{p}}'_i$  is close to  $\tilde{\mathbf{p}}_i$ , we obtain

$$\begin{aligned} \|(\mathbf{A}^T \mathbf{A} + \mathbf{M})^{1/2}(\tilde{\mathbf{p}}'_i - \tilde{\mathbf{p}}_i)\|_2^2 &= (\tilde{\mathbf{p}}'_i - \tilde{\mathbf{p}}_i)^T (\mathbf{A}^T \mathbf{A} + \mathbf{M})(\tilde{\mathbf{p}}'_i - \tilde{\mathbf{p}}_i) \\ &\leq \frac{1}{1-\epsilon} (\tilde{\mathbf{p}}'_i - \tilde{\mathbf{p}}_i)^T (\mathbf{A}^T \mathbf{S}_i^T \mathbf{S}_i \mathbf{A} + \mathbf{M})(\tilde{\mathbf{p}}'_i - \tilde{\mathbf{p}}_i) \leq \frac{\epsilon_0^2}{1-\epsilon} \tilde{\mathbf{p}}_i^T (\mathbf{A}^T \mathbf{S}_i^T \mathbf{S}_i \mathbf{A} + \mathbf{M}) \tilde{\mathbf{p}}_i. \end{aligned}$$

By definition,  $\tilde{\mathbf{p}}_i = (\mathbf{A}^T \mathbf{S}_i^T \mathbf{S}_i \mathbf{A} + \mathbf{M})^{-1} \tilde{\mathbf{p}}_i$ , it follows that

$$\begin{aligned} &\|(\mathbf{A}^T \mathbf{A} + \mathbf{M})^{1/2}(\tilde{\mathbf{p}}'_i - \tilde{\mathbf{p}}_i)\|_2^2 \\ &\leq \frac{\epsilon_0^2}{1-\epsilon} \mathbf{c}^T \mathbf{A} (\mathbf{A}^T \mathbf{S}_i^T \mathbf{S}_i \mathbf{A} + \mathbf{M})^{-1} (\mathbf{A}^T \mathbf{S}_i^T \mathbf{S}_i \mathbf{A} + \mathbf{M}) (\mathbf{A}^T \mathbf{S}_i^T \mathbf{S}_i \mathbf{A} + \mathbf{M})^{-1} \mathbf{A}^T \mathbf{c} \\ &= \frac{\epsilon_0^2}{1-\epsilon} \mathbf{c}^T \mathbf{A} (\mathbf{A}^T \mathbf{S}_i^T \mathbf{S}_i \mathbf{A} + \mathbf{M})^{-1} \mathbf{A}^T \mathbf{c} \\ &\leq \frac{\epsilon_0^2}{(1-\epsilon)^2} \mathbf{c}^T \mathbf{A} (\mathbf{A}^T \mathbf{A} + \mathbf{M})^{-1} \mathbf{A}^T \mathbf{c} \\ &= \frac{\epsilon_0^2}{(1-\epsilon)^2} \|(\mathbf{A}^T \mathbf{A} + \mathbf{M})^{1/2} \mathbf{p}^*\|_2^2. \end{aligned}$$

It follows from the triangle inequality that

$$\begin{aligned} &\|(\mathbf{A}^T \mathbf{A} + \mathbf{M})^{1/2}(\tilde{\mathbf{p}}' - \mathbf{p}^*)\|_2 \leq \|(\mathbf{A}^T \mathbf{A} + \mathbf{M})^{1/2}(\tilde{\mathbf{p}} - \mathbf{p}^*)\|_2 + \|(\mathbf{A}^T \mathbf{A} + \mathbf{M})^{1/2}(\tilde{\mathbf{p}}' - \tilde{\mathbf{p}})\|_2 \\ &= \|(\mathbf{A}^T \mathbf{A} + \mathbf{M})^{1/2}(\tilde{\mathbf{p}} - \mathbf{p}^*)\|_2 + \left\| \frac{1}{m} \sum_{i=1}^m (\mathbf{A}^T \mathbf{A} + \mathbf{M})^{1/2}(\tilde{\mathbf{p}}'_i - \tilde{\mathbf{p}}_i) \right\|_2 \\ &\leq \|(\mathbf{A}^T \mathbf{A} + \mathbf{M})^{1/2}(\tilde{\mathbf{p}} - \mathbf{p}^*)\|_2 + \frac{1}{m} \sum_{i=1}^m \|(\mathbf{A}^T \mathbf{A} + \mathbf{M})^{1/2}(\tilde{\mathbf{p}}'_i - \tilde{\mathbf{p}}_i)\|_2 \\ &\leq \|(\mathbf{A}^T \mathbf{A} + \mathbf{M})^{1/2}(\tilde{\mathbf{p}} - \mathbf{p}^*)\|_2 + \frac{\epsilon_0}{1-\epsilon} \|(\mathbf{A}^T \mathbf{A} + \mathbf{M})^{1/2} \mathbf{p}^*\|_2 \\ &\leq \left( \vartheta \frac{\epsilon}{m} + \vartheta \frac{\epsilon^2}{1-\epsilon} + \frac{\epsilon_0}{1-\epsilon} \right) \|(\mathbf{A}^T \mathbf{A} + \mathbf{M})^{1/2} \mathbf{p}^*\|_2, \end{aligned}$$

where the last inequality follows from (28). Finally, by (29), we obtain

$$\begin{aligned} \phi(\tilde{\mathbf{p}}') - \phi(\mathbf{p}^*) &= \|(\mathbf{A}^T \mathbf{A} + \mathbf{M})^{1/2}(\tilde{\mathbf{p}}' - \mathbf{p}^*)\|_2^2 \\ &\leq \left( \vartheta \frac{\epsilon}{m} + \vartheta \frac{\epsilon^2}{1-\epsilon} + \frac{\epsilon_0}{1-\epsilon} \right)^2 \|(\mathbf{A}^T \mathbf{A} + \mathbf{M})^{1/2} \mathbf{p}^*\|_2^2 \\ &= - \left( \vartheta \frac{\epsilon}{m} + \vartheta \frac{\epsilon^2}{1-\epsilon} + \frac{\epsilon_0}{1-\epsilon} \right)^2 \phi(\mathbf{p}^*), \end{aligned}$$

by which the lemma follows.

## Appendix F. Proof of Lemma 10 (Convergence of GIANT)

Recall the definitions:  $\phi_t(\mathbf{p}) \triangleq \mathbf{p}^T \mathbf{H}_t \mathbf{p} - 2\mathbf{g}_t^T \mathbf{p}$ ,  $\mathbf{w}_{t+1} = \mathbf{w}_t - \tilde{\mathbf{p}}_t$ ,  $\Delta_t = \mathbf{w}_t - \mathbf{w}^*$ , and  $\Delta_{t+1} = \mathbf{w}_{t+1} - \mathbf{w}^*$ . It holds that

$$\tilde{\mathbf{p}}_t = \mathbf{w}_t - \mathbf{w}_{t+1} = \Delta_t - \Delta_{t+1}.$$

It follows that

$$\begin{aligned}\phi_t(\tilde{\mathbf{p}}_t) &= (\mathbf{\Delta}_t - \mathbf{\Delta}_{t+1})^T \mathbf{H}_t (\mathbf{\Delta}_t - \mathbf{\Delta}_{t+1}) - 2(\mathbf{\Delta}_t - \mathbf{\Delta}_{t+1})^T \mathbf{g}_t, \\ (1 - \alpha^2) \cdot \phi_t\left(\frac{1}{1-\alpha^2} \mathbf{\Delta}_t\right) &= \frac{1}{1-\alpha^2} \mathbf{\Delta}_t^T \mathbf{H}_t \mathbf{\Delta}_t - 2\mathbf{\Delta}_t^T \mathbf{g}_t.\end{aligned}$$

By taking the difference between the above two equations, we obtain

$$\begin{aligned}\phi_t(\tilde{\mathbf{p}}_t) - (1 - \alpha^2) \phi_t\left(\frac{1}{1-\alpha^2} \mathbf{\Delta}_t\right) \\ = \mathbf{\Delta}_{t+1}^T \mathbf{H}_t \mathbf{\Delta}_{t+1} - 2\mathbf{\Delta}_t^T \mathbf{H}_t \mathbf{\Delta}_{t+1} + 2\mathbf{\Delta}_{t+1}^T \mathbf{g}_t - \frac{\alpha^2}{1-\alpha^2} \mathbf{\Delta}_t^T \mathbf{H}_t \mathbf{\Delta}_t.\end{aligned}$$

By assumption, it holds that

$$\phi_t(\tilde{\mathbf{p}}_t) \leq (1 - \alpha^2) \min_{\mathbf{p}} \phi_t(\mathbf{p}) \leq (1 - \alpha^2) \phi_t\left(\frac{1}{1-\alpha^2} \mathbf{\Delta}_t\right),$$

and thereby

$$\mathbf{\Delta}_{t+1}^T \mathbf{H}_t \mathbf{\Delta}_{t+1} - 2\mathbf{\Delta}_t^T \mathbf{H}_t \mathbf{\Delta}_{t+1} + 2\mathbf{\Delta}_{t+1}^T \mathbf{g}_t - \frac{\alpha^2}{1-\alpha^2} \mathbf{\Delta}_t^T \mathbf{H}_t \mathbf{\Delta}_t \leq 0. \quad (30)$$

We can write  $\mathbf{g}_t \triangleq \mathbf{g}(\mathbf{w}_t)$  by

$$\begin{aligned}\mathbf{g}(\mathbf{w}_t) &= \mathbf{g}(\mathbf{w}^*) + \left( \int_0^1 \mathbf{H}(\mathbf{w}^* + \tau(\mathbf{w}_t - \mathbf{w}^*)) d\tau \right) (\mathbf{w}_t - \mathbf{w}^*) \\ &= \left( \int_0^1 \mathbf{H}(\mathbf{w}^* + \tau(\mathbf{w}_t - \mathbf{w}^*)) d\tau \right) \mathbf{\Delta}_t,\end{aligned}$$

where the latter equality follows from that  $\mathbf{g}(\mathbf{w}^*) = \mathbf{0}$ . It follows that

$$\begin{aligned}\left\| \mathbf{H}_t \mathbf{\Delta}_t - \mathbf{g}(\mathbf{w}_t) \right\|_2 &\leq \left\| \mathbf{\Delta}_t \right\|_2 \left\| \int_0^1 \left[ \mathbf{H}(\mathbf{w}_t) - \mathbf{H}(\mathbf{w}^* + \tau(\mathbf{w}_t - \mathbf{w}^*)) \right] d\tau \right\|_2 \\ &\leq \left\| \mathbf{\Delta}_t \right\|_2 \int_0^1 \left\| \mathbf{H}(\mathbf{w}_t) - \mathbf{H}(\mathbf{w}^* + \tau(\mathbf{w}_t - \mathbf{w}^*)) \right\|_2 d\tau \\ &\leq \left\| \mathbf{\Delta}_t \right\|_2 \int_0^1 (1 - \tau)L \left\| \mathbf{w}_t - \mathbf{w}^* \right\|_2 d\tau \\ &= \frac{L}{2} \left\| \mathbf{\Delta}_t \right\|_2^2.\end{aligned} \quad (31)$$

Here the second inequality follows from Jensen's inequality; the third inequality follows from the assumption of  $L$ -Lipschitz. It follows from (30) and (31) that

$$\begin{aligned}\mathbf{\Delta}_{t+1}^T \mathbf{H}_t \mathbf{\Delta}_{t+1} &\leq 2\mathbf{\Delta}_{t+1}^T (\mathbf{H}_t \mathbf{\Delta}_t - \mathbf{g}_t) + \frac{\alpha^2}{1-\alpha^2} \mathbf{\Delta}_t^T \mathbf{H}_t \mathbf{\Delta}_t \\ &\leq L \left\| \mathbf{\Delta}_{t+1} \right\|_2 \left\| \mathbf{\Delta}_t \right\|_2^2 + \frac{\alpha^2}{1-\alpha^2} \mathbf{\Delta}_t^T \mathbf{H}_t \mathbf{\Delta}_t,\end{aligned}$$

by which the lemma follows.

## References

- Dimitris Achlioptas. Database-friendly random projections: Johnson-Lindenstrauss with binary coins. *Journal of computer and System Sciences*, 66(4):671–687, 2003. [10](#), [39](#)
- Keith Bonawitz, Vladimir Ivanov, Ben Kreuter, Antonio Marcedone, H Brendan McMahan, Sarvar Patel, Daniel Ramage, Aaron Segal, and Karn Seth. Practical secure aggregation for privacy preserving machine learning. *IACR Cryptology ePrint Archive*, 2017:281, 2017. [2](#)
- Stephen Boyd, Neal Parikh, Eric Chu, Borja Peleato, and Jonathan Eckstein. Distributed optimization and statistical learning via the alternating direction method of multipliers. *Foundations and Trends® in Machine Learning*, 3(1):1–122, 2011. [3](#)
- Christopher JC Burges. A tutorial on support vector machines for pattern recognition. *Data mining and knowledge discovery*, 2(2):121–167, 1998.
- Olivier Chapelle. Training a support vector machine in the primal. *Neural Computation*, 19(5):1155–1178, 2007.
- Kenneth L. Clarkson and David P. Woodruff. Low rank approximation and regression in input sparsity time. In *Annual ACM Symposium on theory of computing (STOC)*, 2013. [10](#)
- Jeffrey Dean and Sanjay Ghemawat. MapReduce: simplified data processing on large clusters. *Communications of the ACM*, 51(1):107–113, 2008. [2](#)
- Aditya Devarakonda, Kimon Fountoulakis, James Demmel, and Michael W Mahoney. Avoiding communication in primal and dual block coordinate descent methods. *arXiv preprint arXiv:1612.04003*, 2016. [3](#)
- Petros Drineas and Michael W Mahoney. RandNLA: randomized numerical linear algebra. *Communications of the ACM*, 59(6):80–90, 2016. [10](#)
- Petros Drineas, Ravi Kannan, and Michael W. Mahoney. Fast Monte Carlo algorithms for matrices I: Approximating matrix multiplication. *SIAM Journal on Computing*, 36(1):132–157, 2006a. [8](#)
- Petros Drineas, Michael W. Mahoney, and S. Muthukrishnan. Sampling algorithms for  $\ell_2$  regression and applications. In *Annual ACM-SIAM Symposium on Discrete Algorithm (SODA)*, 2006b. [19](#), [39](#)
- Petros Drineas, Michael W. Mahoney, S. Muthukrishnan, and Tamás Sarlós. Faster least squares approximation. *Numerische Mathematik*, 117(2):219–249, 2011. [10](#), [19](#), [39](#)
- Petros Drineas, Malik Magdon-Ismail, Michael W. Mahoney, and David P. Woodruff. Fast approximation of matrix coherence and statistical leverage. *Journal of Machine Learning Research*, 13:3441–3472, 2012. [9](#), [10](#), [39](#)
- Olivier Fercoq and Peter Richtárik. Optimization in high dimensions via accelerated, parallel, and proximal coordinate descent. *SIAM Review*, 58(4):739–771, 2016. [2](#)

- Gene H Golub and Charles F Van Loan. *Matrix computations*, volume 3. JHU Press, 2012. [41](#)
- Martin Jaggi, Virginia Smith, Martin Takáč, Jonathan Terhorst, Sanjay Krishnan, Thomas Hofmann, and Michael I Jordan. Communication-efficient distributed dual coordinate ascent. In *Advances in Neural Information Processing Systems (NIPS)*, 2014. [3](#), [18](#)
- Rie Johnson and Tong Zhang. Accelerating stochastic gradient descent using predictive variance reduction. In *Advances in Neural Information Processing Systems (NIPS)*, 2013. [32](#), [36](#)
- William B. Johnson and Joram Lindenstrauss. Extensions of Lipschitz mappings into a Hilbert space. *Contemporary mathematics*, 26(189-206), 1984. [10](#), [39](#)
- S. Sathiya Keerthi and Dennis DeCoste. A modified finite Newton method for fast solution of large scale linear SVMs. In *Journal of Machine Learning Research*, pages 341–361, 2005.
- Jakub Konečný, H Brendan McMahan, Daniel Ramage, and Peter Richtárik. Federated optimization: distributed machine learning for on-device intelligence. *arXiv preprint arXiv:1610.02527*, 2016a. [2](#)
- Jakub Konečný, H Brendan McMahan, Felix X Yu, Peter Richtárik, Ananda Theertha Suresh, and Dave Bacon. Federated learning: strategies for improving communication efficiency. *arXiv preprint arXiv:1610.05492*, 2016b. [2](#)
- Jason D Lee, Qihang Lin, Tengyu Ma, and Tianbao Yang. Distributed stochastic variance reduced gradient methods and a lower bound for communication complexity. *arXiv preprint arXiv:1507.07595*, 2015. [2](#)
- Mu Li, David G Andersen, Jun Woo Park, Alexander J Smola, Amr Ahmed, Vanja Josifovski, James Long, Eugene J Shekita, and Bor-Yiing Su. Scaling distributed machine learning with the parameter server. In *USENIX Symposium on Operating Systems Design and Implementation (OSDI)*, 2014. [2](#)
- Ji Liu, Stephen J Wright, Christopher Ré, Victor Bittorf, and Srikrishna Sridhar. An asynchronous parallel stochastic coordinate descent algorithm. *Journal of Machine Learning Research*, 16(285-322):1–5, 2015. [2](#)
- Yucheng Low, Danny Bickson, Joseph Gonzalez, Carlos Guestrin, Aapo Kyrola, and Joseph M. Hellerstein. Distributed GraphLab: A framework for machine learning and data mining in the cloud. *Proceedings of the VLDB Endowment*, 2012. [2](#)
- Yichao Lu, Paramveer Dhillon, Dean P Foster, and Lyle Ungar. Faster ridge regression via the subsampled randomized Hadamard transform. In *Advances in Neural Information Processing Systems (NIPS)*, 2013. [10](#), [39](#)
- Chenxin Ma, Virginia Smith, Martin Jaggi, Michael Jordan, Peter Richtarik, and Martin Takac. Adding vs. averaging in distributed primal-dual optimization. In *International Conference on Machine Learning (ICML)*, 2015. [3](#), [18](#), [30](#)

- Ping Ma, Michael Mahoney, and Bin Yu. A statistical perspective on algorithmic leveraging. In *International Conference on Machine Learning (ICML)*, 2014. 19, 20
- Dhruv Mahajan, S Sathiya Keerthi, S Sundararajan, and Léon Bottou. A parallel SGD method with strong convergence. *arXiv preprint arXiv:1311.0636*, 2013. 2
- Michael W. Mahoney. Randomized algorithms for matrices and data. *Foundations and Trends in Machine Learning*, 3(2):123–224, 2011. 8, 10, 19
- Olvi L Mangasarian. A finite Newton method for classification. *Optimization Methods and Software*, 17(5):913–929, 2002.
- Peter McCullagh and John A. Nelder. *Generalized linear models*, volume 37. CRC press, 1989.
- Brendan McMahan, Eider Moore, Daniel Ramage, Seth Hampson, and Blaise Agueray Arcas. Communication-efficient learning of deep networks from decentralized data. In *International Conference on Artificial Intelligence and Statistics (AISTATS)*, 2017. 2
- Xiangrui Meng and Michael W Mahoney. Low-distortion subspace embeddings in input-sparsity time and applications to robust linear regression. In *Annual ACM Symposium on Theory of Computing (STOC)*, 2013. 10
- Xiangrui Meng, Joseph Bradley, Burak Yavuz, Evan Sparks, Shivaram Venkataraman, Davies Liu, Jeremy Freeman, DB Tsai, Manish Amde, Sean Owen, et al. MLlib: machine learning in Apache Spark. *Journal of Machine Learning Research*, 17(34):1–7, 2016. 2
- Ion Necoara and Dragos Clipici. Parallel random coordinate descent method for composite minimization: Convergence analysis and error bounds. *SIAM Journal on Optimization*, 26(1):197–226, 2016. 2
- John Nelson and Huy L Nguyễn. OSNAP: Faster numerical linear algebra algorithms via sparser subspace embeddings. In *IEEE Annual Symposium on Foundations of Computer Science (FOCS)*, 2013. 10
- Jorge Nocedal and Stephen Wright. *Numerical optimization*. Springer Science & Business Media, 2006. 6, 11
- Mert Pilanci and Martin J Wainwright. Iterative Hessian sketch: Fast and accurate solution approximation for constrained least-squares. *Journal of Machine Learning Research*, pages 1–33, 2015. 8
- Mert Pilanci and Martin J Wainwright. Newton sketch: A near linear-time optimization algorithm with linear-quadratic convergence. *SIAM Journal on Optimization*, 27(1):205–245, 2017. 7, 8
- Boris T Polyak. Newtons method and its use in optimization. *European Journal of Operational Research*, 181(3):1086–1096, 2007. 11
- Ali Rahimi and Benjamin Recht. Random features for large-scale kernel machines. In *Advances in Neural Information Processing Systems (NIPS)*, 2007. 21, 26

- Benjamin Recht, Christopher Re, Stephen Wright, and Feng Niu. Hogwild: a lock-free approach to parallelizing stochastic gradient descent. In *Advances in Neural Information Processing Systems (NIPS)*, 2011. [2](#)
- Sashank J Reddi, Ahmed Hefny, Suvrit Sra, Barnabas Poczos, and Alexander J Smola. On variance reduction in stochastic gradient descent and its asynchronous variants. In *Advances in Neural Information Processing Systems (NIPS)*. 2015. [2](#)
- Sashank J Reddi, Jakub Konecný, Peter Richtárik, Barnabás Póczós, and Alex Smola. AIDE: fast and communication efficient distributed optimization. *arXiv preprint arXiv:1608.06879*, 2016. [3](#), [7](#), [18](#), [21](#), [24](#), [25](#), [30](#), [31](#), [36](#)
- Peter Richtárik and Martin Takác. Distributed coordinate descent method for learning with big data. *Journal of Machine Learning Research*, 17(1):2657–2681, 2016. [2](#)
- Peter Richtárik and Martin Takávc. Parallel coordinate descent methods for big data optimization. *Mathematical Programming*, 156(1-2):433–484, 2016. [2](#)
- Farbod Roosta-Khorasani. *Randomized algorithms for solving large scale nonlinear least squares problems*. PhD thesis, University of British Columbia, 2015. [11](#)
- Farbod Roosta-Khorasani and Michael W Mahoney. Sub-sampled Newton methods I: globally convergent algorithms. *arXiv preprint arXiv:1601.04737*, 2016a. [3](#), [11](#), [24](#), [35](#)
- Farbod Roosta-Khorasani and Michael W Mahoney. Sub-sampled Newton methods II: Local convergence rates. *arXiv preprint arXiv:1601.04738*, 2016b. [3](#), [7](#), [8](#), [24](#)
- Farbod Roosta-Khorasani, Kees van den Doel, and Uri Ascher. Stochastic algorithms for inverse problems involving PDEs and many measurements. *SIAM J. Scientific Computing*, 36(5):S3–S22, 2014a. doi: 10.1137/130922756. [11](#)
- Farbod Roosta-Khorasani, Kees van den Doel, and Uri Ascher. Data completion and stochastic algorithms for PDE inversion problems with many measurements. *Electronic Transactions on Numerical Analysis*, 42:177–196, 2014b. [11](#)
- Farbod Roosta-Khorasani, Gábor J. Székely, and Uri Ascher. Assessing stochastic algorithms for large scale nonlinear least squares problems using extremal probabilities of linear combinations of gamma random variables. *SIAM/ASA Journal on Uncertainty Quantification*, 3(1):61–90, 2015. [11](#)
- Bernhard Schölkopf and Alexander J. Smola. *Learning with Kernels: Support Vector Machines, Regularization, Optimization, and Beyond*. MIT Press, 2002.
- Shai Shalev-Shwartz and Shai Ben-David. *Understanding machine learning: from theory to algorithms*. Cambridge University Press, 2014. [4](#)
- Ohad Shamir and Nathan Srebro. Distributed stochastic optimization and learning. In *Annual Allerton Conference on Communication, Control, and Computing*, 2014. [2](#)

- Ohad Shamir, Nati Srebro, and Tong Zhang. Communication-efficient distributed optimization using an approximate Newton-type method. In *International conference on machine learning (ICML)*, 2014. [3](#), [7](#), [8](#), [18](#), [21](#), [24](#), [25](#), [30](#), [36](#)
- Virginia Smith, Simone Forte, Chenxin Ma, Martin Takac, Michael I Jordan, and Martin Jaggi. CoCoA: A general framework for communication-efficient distributed optimization. *arXiv preprint arXiv:1611.02189*, 2016. [3](#), [7](#), [18](#), [25](#)
- Virginia Smith, Chao-Kai Chiang, Maziar Sanjabi, and Ameet Talwalkar. Federated multi-task learning. *arXiv preprint arXiv:1705.10467*, 2017. [2](#)
- Joel A Tropp. Improved analysis of the subsampled randomized hadamard transform. *Advances in Adaptive Data Analysis*, 3(01n02):115–126, 2011. [10](#), [39](#)
- Joel A Tropp. An introduction to matrix concentration inequalities. *arXiv preprint arXiv:1501.01571*, 2015. [8](#)
- Leslie G. Valiant. A bridging model for parallel computation. *Communications of the ACM*, 33(8):103–111, 1990. [15](#)
- Vladimir N. Vapnik. *Statistical learning theory*, volume 1. Wiley New York, 1998.
- Shusen Wang, Luo Luo, and Zhihua Zhang. SPSD matrix approximation via column selection: Theories, algorithms, and extensions. *Journal of Machine Learning Research*, 17(49):1–49, 2016. [19](#), [39](#)
- Shusen Wang, Alex Gittens, and Michael W. Mahoney. Sketched ridge regression: Optimization perspective, statistical perspective, and model averaging. In *International Conference on Machine Learning (ICML)*, 2017. [8](#), [15](#), [19](#), [38](#), [39](#)
- David P Woodruff. Sketching as a tool for numerical linear algebra. *Foundations and Trends® in Theoretical Computer Science*, 10(1–2):1–157, 2014. [8](#), [10](#), [19](#), [39](#)
- Kristian Woodsend and Jacek Gondzio. Exploiting separability in large-scale linear support vector machine training. *Computational Optimization and Applications*, 49(2):241–269, 2011.
- Stephen Wright and Jorge Nocedal. Numerical optimization. *Springer Science*, 35:67–68, 1999. [39](#)
- Peng Xu, Jiyan Yang, Farbod Roosta-Khorasani, Christopher Ré, and Michael W Mahoney. Sub-sampled Newton methods with non-uniform sampling. In *Advances in Neural Information Processing Systems (NIPS)*, 2016. [7](#), [8](#), [24](#)
- Peng Xu, Farbod Roosta-Khorasani, and Michael W Mahoney. Newton-type methods for non-convex optimization under inexact hessian information. *arXiv preprint arXiv:1708.07164*, 2017a. [3](#), [11](#)
- Peng Xu, Farbod Roosta-Khorasani, and Michael W Mahoney. Second-order optimization for non-convex machine learning: An empirical study. *arXiv preprint arXiv:1708.07827*, 2017b. [3](#), [11](#)

- Jiyan Yang, Xiangrui Meng, and Michael W Mahoney. Implementing randomized matrix algorithms in parallel and distributed environments. *Proceedings of the IEEE*, 104(1): 58–92, 2016. 8, 20
- Tianbao Yang. Trading computation for communication: distributed stochastic dual coordinate ascent. In *Advances in Neural Information Processing Systems (NIPS)*, 2013. 2
- Matei Zaharia, Mosharaf Chowdhury, Michael J Franklin, Scott Shenker, and Ion Stoica. Spark: Cluster computing with working sets. *HotCloud*, 10(10-10):95, 2010. 2
- Yuchen Zhang and Xiao Lin. DiSCO: distributed optimization for self-concordant empirical loss. In *International Conference on Machine Learning (ICML)*, 2015. 3, 7, 25, 30
- Yuchen Zhang, John C. Duchi, and Martin J. Wainwright. Communication-efficient algorithms for statistical optimization. *Journal of Machine Learning Research*, 14:3321–3363, 2013. 15, 33
- Shun Zheng, Fen Xia, Wei Xu, and Tong Zhang. A general distributed dual coordinate optimization framework for regularized loss minimization. *arXiv preprint arXiv:1604.03763*, 2016. 2
- Martin Zinkevich, Markus Weimer, Lihong Li, and Alex J Smola. Parallelized stochastic gradient descent. In *Advances in Neural Information Processing Systems (NIPS)*, 2010. 2